Model-based trajectory planning, optimization, and open-loop control of a continuous slab reheating furnace

authored by **A. Steinboeck, K. Graichen, D. Wild, T. Kiefer, and A. Kugi**

and published in *Journal of Process Control*.

Cite this article as:

A. Steinboeck, K. Graichen, D. Wild, T. Kiefer, and A. Kugi, "Model-based trajectory planning, optimization, and open-loop control of a continuous slab reheating furnace", *Journal of Process Control*, vol. 21, no. 2, pp. 279–292, 2011.
DOI: 10.1016/j.jprocont.2010.08.004

BibTex entry:

```
@ARTICLE{steinboeck11b,
  AUTHOR = {Steinboeck, A. and Graichen, K. and Wild, D. and Kiefer, T. and Kugi, A.},
  TITLE = {Model-based trajectory planning, optimization, and open-loop control of a continuous slab
      reheating furnace},
  JOURNAL = {Journal of Process Control},
  YEAR = {2011},
  volume = {21},
  number = {2},
  pages = {279-292},
  doi = {10.1016/j.jprocont.2010.08.004},
  url = {http://www.sciencedirect.com/science/article/pii/S0959152410001800}
}
```

Link to original paper:

http://dx.doi.org/10.1016/j.jprocont.2010.08.004
http://www.sciencedirect.com/science/article/pii/S0959152410001800

Contact:

Automation and Control Institute (ACIN)
Vienna University of Technology
Gusshausstrasse 27-29/E376
1040 Vienna, Austria

Internet: www.acin.tuwien.ac.at
E-mail: office@acin.tuwien.ac.at
Phone: +43 1 58801 37601
Fax: +43 1 58801 37699

Model-based trajectory planning, optimization, and open-loop control of a continuous slab reheating furnace

A. Steinboeck*[,a], K. Graichen[a], D. Wild[b], T. Kiefer[b], A. Kugi[a]

[a]*Automation and Control Institute, Vienna University of Technology, Gusshausstrasse 27–29, 1040 Wien, Austria*
[b]*AG der Dillinger Hüttenwerke, Werkstrasse 1, 66763 Dillingen/Saar, Germany*

Abstract

A temperature control method is developed for reheating steel slabs in an industrial furnace. The work was motivated by the need for mathematically simple furnace control schemes that feature accuracy, robustness, applicability to online control, and capabilities of non-steady-state operating scenarios, where the temperature goals and other properties of the slabs may vary considerably. The proposed hierarchical control concept computes desired heat inputs for each individual slab based on a discrete-time nonlinear model. Then, a quadratic program is solved to plan reference trajectories of furnace temperatures which optimally realize the desired heat inputs into the slabs. The iterative algorithm accounts for constraints on system inputs as well as states and may be used for open-loop control or as a feedforward branch in two-degrees-of-freedom control structures. The feasibility and the limitations of the approach are demonstrated by means of an example problem.

Key words: Reheating furnace for steel slabs, nonlinear discontinuous dynamical system, open-loop control, trajectory planning, quadratic programming, non-steady-state operation

1. Introduction

1.1. Slab reheating furnaces

The metal industry uses various types of furnaces for heat treatment or reheating, i. e., as a preparation for hot working. The *energy consumption*, the *processing costs*, the *overall throughput*, and the *product quality* are key performance indicators for the control of such industrial furnaces. The furnaces can be classified as nonlinear, distributed parameter systems with multiple inputs and outputs and usually discontinuous time dependence. Moreover, interdependencies of physical quantities are sometimes not clear-cut.

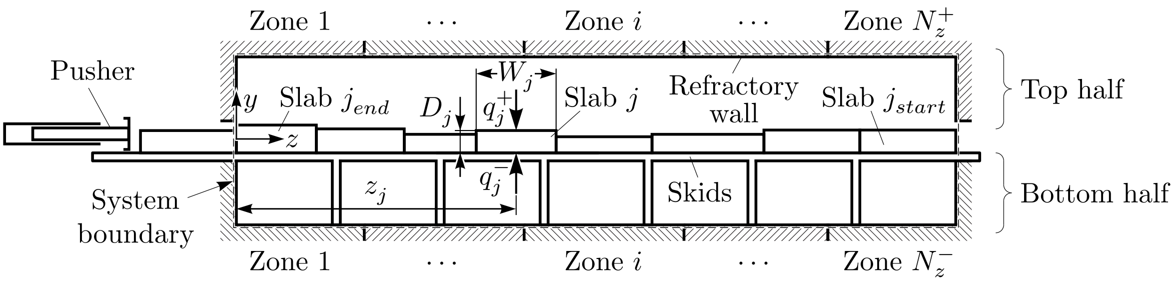

Figure 1: Sectional view of a pusher-type slab reheating furnace (not to scale, symbols explained in Subsection 2).

*Corresponding author. *Tel.:* +43 1 58801 77629, *fax:* +43 1 58801 37699.
Email address: andreas.steinboeck@tuwien.ac.at (A. Steinboeck)

Post-print version of the article: A. Steinboeck, K. Graichen, D. Wild, T. Kiefer, and A. Kugi, "Model-based trajectory planning, optimization, and open-loop control of a continuous slab reheating furnace", *Journal of Process Control*, vol. 21, no. 2, pp. 279–292, 2011. DOI: 10.1016/j.jprocont.2010.08.004
The content of this post-print version is identical to the published paper but without the publisher's final layout or copy editing.

This paper presents a model-based process control scheme of fuel-fired continuous furnaces for reheating steel slabs before working in a hot rolling mill. However, the approach is equally applicable to furnaces for billets, bars, or similar products and can be adapted for other furnace types.

In a continuous slab reheating furnace, slabs are conveyed through the furnace interior while being reheated. A *pusher-type* slab reheating furnace, as considered in this analysis, is outlined in Figure 1. The slabs are arranged in a single or several parallel rows and pushed in the longitudinally direction through the furnace. They slide on skids to enable their reheating from both the bottom and the top side. The term *continuous* is somewhat misleading because the slab movement itself is discontinuous.

The temperature distribution *inside* the slabs is a highly important but not measurable system quantity. Therefore, temperature readings from thermocouples being installed in the refractory furnace walls [1–11] may be utilized for estimating unknown slab temperatures by observers [12].

1.2. Furnace control task

Frequently, the furnace operation is governed by *supervisory plant control* that defines the order of the slabs, their movement, and their desired final temperature profile, which is considered homogeneous in this analysis. In terms of temperature control, only the supply rates of fuel and combustion air to the burners serve as controllable inputs. The (sometimes antagonistic) objectives of an industrial furnace control scheme are:

- Minimum deviation between the desired and the realized final slab temperature profiles
- Minimum specific energy consumption $= \dfrac{\text{Energy supplied by fuel}}{\text{Mass of reheated material}}$
- Minimum loss of material through oxidization (scale formation)
- Minimum decarburization depth (may impair the material quality)

These control objectives are stimulated by economical reasons, in particular energy costs and ever-increasing demands in terms of quality and diversification of products. The control task is greatly determined by the discontinuous nature of the furnace process. Apart from the non-steady-state flow of slabs, they may vary significantly in size, steel grade, material properties, initial temperature, desired final temperature, available reheating time, path-time diagram, and monetary value (cf. [1, 4, 9, 13–16]). Therefore, multiple probably incompatible control objectives are to be reached. For instance, if the difference between the desired final temperature of neighboring slabs is too large, the control problem may be not feasible.

Furnace control should additionally account for *constraints* like:

- Construction and geometry of the furnace including type and arrangement of heat sources (burners) and heat sinks (slabs, furnace walls, skids, etc.)
- Protection of the furnace against immoderate wear
- Constraints on the temperatures of the furnace walls in order to protect them from damage
- Limitations of the manipulated variables, i. e., fuel and air feeds
- Metallurgical constraints of the slab temperature trajectories
- Unforeseen standstills or delays caused by upstream or downstream process steps

Especially, the restrictions on the manipulated variables and the furnace wall temperatures can limit the control performance. If such constraints are active, controllability of the corresponding quantities may be lost—at least temporarily.

1.3. Existing control schemes

Generally, it may be distinguished between control strategies that regulate exclusively the temperature or the velocity of the material to be reheated [17] or both [6, 9, 11, 16, 18–20]. Temperature control systems may either control slab temperatures directly or indirectly by regulating furnace temperatures as intermediate quantities. The latter strategy is adopted in [2, 21] and in this paper. It may be classified as *open-loop control* of slab temperatures, since there is no feedback from (estimated or measured) slab temperatures.

Post-print version of the article: A. Steinboeck, K. Graichen, D. Wild, T. Kiefer, and A. Kugi, "Model-based trajectory planning, optimization, and open-loop control of a continuous slab reheating furnace", *Journal of Process Control*, vol. 21, no. 2, pp. 279–292, 2011. doi: 10.1016/j.jprocont.2010.08.004

Reference signals of furnace temperatures are commanded to some subordinate (feedback) control devices, which regulate the supply of fuel and combustion air.

Several control schemes, e. g., [1–4, 6, 8, 11, 18, 21–23], have been developed for steady-state furnace operation or are based on steady-state furnace models, meaning that all slabs have equal properties (geometry, material, initial temperature, desired final temperature, residence time in the furnace, etc.) and that the slabs are moved forward at regular time intervals. Clearly, if these controllers are used to operate the system under non-steady-state conditions, the control performance may suffer.

Most furnace temperature control systems are based on some sort of modular control, mainly *hierarchical* (open-loop) or *cascaded* (closed-loop) control structures [4–6, 9–11, 13, 14, 18, 19, 21, 24–28]. In cascaded structures, the inner loops are usually controlling the furnace temperature, for instance by PI or PID controllers [4, 10, 11, 13, 24–26, 28].

Some control concepts utilize table look-up algorithms with setpoints of furnace zone temperatures being stored in databases [1, 2, 4, 6, 9, 11, 15, 16, 22]. The tabulated data can be determined off-line using steady-state planning and optimization algorithms or empirically from operators' experiences.

The control task is simplified if the dynamic interaction between the zones is neglected [2–4, 10, 24, 29, 30]. The idea of *zone-based* feedback control (cf. [3, 7, 15, 24, 25]) is that the slabs should reach predefined (optimal) temperature setpoint values (at the end of the furnace zones). The feedback controller either defines setpoints for the zone temperature [5, 9, 10, 13, 15, 24, 25, 30] or straightaway for the heat input (fuel supply) to the respective zone [3, 20]. Alternatively, the control error may be used in a static optimization problem to select optimum zone temperatures [7].

For two-degrees-of-freedom control, the output of feedback controllers is added to preplanned (optimal) furnace temperature trajectories [6, 8, 10, 11, 22] or preplanned fuel flow rates [16]. Usually, the feedback law is based on the control error of the slab temperature, which, therefore, has to be estimated by some observer. For a single furnace zone, [29] presents a nonlinear feedback control law ensuring asymptotic stability.

Surface temperatures measured by pyrometry after the furnace or after the first roughing mill are used for feedback control in [1, 7, 9, 10, 14, 16, 23]. The control performance can be limited because of both the temperature drop and the time delay from the furnace exit to the measuring point. These effects may cause oscillations in the closed loop [7, 10].

Moreover, dynamic optimization can be used to derive optimal fuel flow rates under non-steady-state (transient) conditions [31]. *Model predictive control* (cf. [5, 18, 19, 26, 32, 33]) requires to solve optimization problems in the closed loop, i. e., in real time. Therefore, such algorithms usually rely on simple dynamical models.

1.4. Motivation

Most furnace control strategies, including those mentioned above, are either computationally demanding, which makes them unsuitable for online control, or based on simple dynamical models or even steady-state models, which may limit control accuracy. This paper aims to fill this gap by providing a control method

- which is suitable for realtime execution,
- which accounts for the dynamic interaction between furnace zones,
- which properly accounts for nonlinear effects,
- which ensures accurate slab reheating,
- which can cope with non-steady-state furnace operation, i. e., scenarios where the desired final temperatures and other properties of the slabs vary considerably,
- and which ensures compliance with relevant constraints as far as possible.

1.5. Contents

The paper is organized as follows: Section 2 briefly describes a dynamical model of the considered furnace, which is employed in a hierarchical open-loop control scheme outlined in Section 3. The main result of the paper is an iterative trajectory planning and optimization algorithm, which is developed in Section 4. Based on an example problem, Section 5 demonstrates the feasibility and the accuracy of the method.

Post-print version of the article: A. Steinboeck, K. Graichen, D. Wild, T. Kiefer, and A. Kugi, "Model-based trajectory planning, optimization, and open-loop control of a continuous slab reheating furnace", *Journal of Process Control*, vol. 21, no. 2, pp. 279–292, 2011. DOI: 10.1016/j.jprocont.2010.08.004

2. Mathematical models

This analysis utilizes two mathematical models of the considered furnace, each being tailored to its specific purpose. The models are referred to as *comprehensive model* and *reduced model*. The accuracy of both has been verified by measurements with instrumented test slabs that were reheated in the furnace [34].

The *comprehensive model* was presented by *Wild* and coworkers [12, 34]. It is based on radiation, heat, and mass balances and uses the flow rates of fuel and combustion air as inputs. In this analysis, the model is utilized in simulations for verifying the reduced model and for testing planning and optimization algorithms.

Steinboeck et al. [35] proposed a *reduced model* that is mathematically less demanding and therefore suitable for optimization and control applications. It accounts for radiative heat exchange in the furnace and heat conduction inside the slabs. The model is outlined in the following.

2.1. Slab management, geometry, and position

Consider the furnace shown in Figure 1 and let each slab be uniquely identified by an index $j \in \mathbb{N}$. All slabs $j \in J = \{j_{start}, j_{start}+1, \ldots, j_{end}\}$ are currently inside the furnace, where j_{start} refers to the next slab to be withdrawn from the furnace and j_{end} to the last slab that was pushed in. The slab j enters the furnace at the time $t_{j,0}$ and leaves it at the time $t_{j,exit}$. Let $t_{j,0}$ and $t_{j,exit}$ of all slabs be summarized in the series of event times (t_l^s) with $l \in \mathbb{N}$. Therefore, j_{start} and j_{end} are updated according to $j_{start} = j_{start} + 1$ and $j_{end} = j_{end} + 1$ at $t_{j_{start}+1,0}$ and $t_{j_{end},exit}$, respectively. Likewise, the number of slabs $N_s = |J|$ in the furnace is updated upon such events.

In the global frame of reference shown in Figure 1, the center of the slab j has the current z-position z_j. Slabs may only be moved in positive z-direction. Moreover, let y be a *local* coordinate in vertical direction, which is 0 at the center of the respective slab j. The thickness D_j and the width W_j is the extension of the slab along the direction y and z, respectively.

2.2. Continuous-time model

The bottom and the top half of the furnace volume are each divided into 5 zones, i. e., $N_z^- = N_z^+ = 5$ (cf. Figure 1). Henceforth, all quantities belonging to the bottom and the top half are designated by the superscripts $^-$ and $^+$, respectively.

The zone temperatures $\boldsymbol{T}_z^{\mp} = [T_{z,1}^{\mp}, T_{z,2}^{\mp}, \ldots, T_{z,N_z^{\mp}}^{\mp}]^\mathsf{T}$ are assumed to be homogeneously distributed within each zone. They represent a combination of local flue gas temperatures and wall surface temperatures and serve as inputs of the model. Therefore, the inputs directly correspond to measured zone temperatures in the real furnace. Figure 2 shows the structure of the continuous-time model that is detailed in the following.

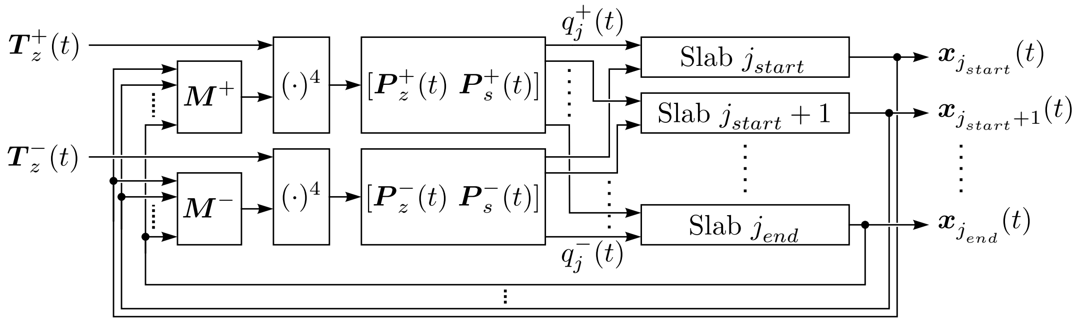

Figure 2: Structure of the continuous-time model.

The heat conduction problem inside the slabs can be solved by means of the Galerkin method with three orthogonal trial functions $h_{j,1}(y) = 1$, $h_{j,2}(y) = 2y/D_j$, and $h_{j,3}(y) = (2y/D_j)^2 - 1/3$. The temperature distribution inside the slab j is approximated as $T_j(y,t) = \sum_{i=1}^{3} x_{j,i}(t) h_{j,i}(y)$, where the so-called Galerkin coefficients $x_{j,i}(t)$, summarized in the state vector $\boldsymbol{x}_j(t) = [x_{j,1}(t), x_{j,2}(t), x_{j,3}(t)]^\mathsf{T}$, reflect the time dependence of the slab temperature. The system dynamics follows as (cf. [35, 36])

$$\dot{\boldsymbol{x}}_j(t) = \boldsymbol{a}_j \boldsymbol{x}_j(t) + \boldsymbol{b}_j^- q_j^-(t) + \boldsymbol{b}_j^+ q_j^+(t) \qquad t > t_{j,0} \tag{1a}$$

Post-print version of the article: A. Steinboeck, K. Graichen, D. Wild, T. Kiefer, and A. Kugi, “Model-based trajectory planning, optimization, and open-loop control of a continuous slab reheating furnace”, *Journal of Process Control*, vol. 21, no. 2, pp. 279–292, 2011. DOI: 10.1016/j.jprocont.2010.08.004
The content of this post-print version is identical to the published paper but without the publisher’s final layout or copy editing.

with the initial value $\boldsymbol{x}_j(t_{j,0}) = \boldsymbol{x}_{j,0}$ corresponding to the initial temperature profile $T_j(y, t_{j,0}) = T_{j,0}(y)$, the expressions

$$\boldsymbol{a}_j = -\frac{12\bar{\lambda}_j(\boldsymbol{x}_j(t))}{\rho_j \bar{c}_j(\boldsymbol{x}_j(t)) D_j^2} \operatorname{diag}\{0 \quad 1 \quad 5\}, \qquad \boldsymbol{b}_j^{\mp} = \frac{1}{\rho_j \bar{c}_j(\boldsymbol{x}_j(t)) D_j} \left[1 \quad \mp 3 \quad {}^{15}\!/_2\right]^{\mathsf{T}}, \tag{1b}$$

the mass density ρ_j, and the net heat flux densities $q_j^-(t)$ and $q_j^+(t)$ into the bottom and top surface of the slab, respectively. The model (1) represents a single slab j as a block on the right hand side of Figure 2. The heat flux densities $q_j^{\mp}(t)$ into the slab j may be interpreted as *intermediate* inputs. The parameters $\bar{c}_j(\boldsymbol{x}_j(t))$ and $\bar{\lambda}_j(\boldsymbol{x}_j(t))$ are weighted mean values of the specific heat capacity c_j and the thermal conductivity λ_j, respectively, which may nonlinearly depend on the local slab temperature [35, 36].

The states $\boldsymbol{x}_j(t)$ have a direct physical interpretation: $x_{j,1}(t)$ is the mean temperature, $x_{j,2}(t)$ defines the asymmetry of the temperature profile, and $x_{j,3}(t)$ corresponds to the symmetric inhomogeneity. Moreover, $T_j(\mp {}^{D_j}\!/_2, t) = [1 \ \mp 1 \ {}^2\!/_3]\boldsymbol{x}_j(t)$ is an acceptable approximation of the surface temperature, which is useful for radiation boundary conditions (cf. (3)).

The heat inputs and the states of all slabs $j \in J$ are summarized in the vectors $\boldsymbol{q}^{\mp}(t) = [q^{\mp}_{j_{start}}(t), q^{\mp}_{j_{start}+1}(t), \ldots, q^{\mp}_{j_{end}}(t)]^{\mathsf{T}}$ and $\boldsymbol{X}(t) = [\boldsymbol{x}^{\mathsf{T}}_{j_{start}}(t), \boldsymbol{x}^{\mathsf{T}}_{j_{start}+1}(t), \ldots, \boldsymbol{x}^{\mathsf{T}}_{j_{end}}(t)]^{\mathsf{T}}$, respectively. Note that their components as well as their dimensions N_s and $3N_s$, respectively, may vary at t_l^s. The model (1a) is assembled for the whole system as (cf. [35])

$$\dot{\boldsymbol{X}}(t) = \left[\delta_{i,j}\boldsymbol{a}_j\right]_{\substack{i=j_{start}\cdots j_{end}\\ j=j_{start}\cdots j_{end}}} \boldsymbol{X}(t) + \left[\delta_{i,j}\boldsymbol{b}_j^-\right]_{\substack{i=j_{start}\cdots j_{end}\\ j=j_{start}\cdots j_{end}}} \boldsymbol{q}^-(t) + \left[\delta_{i,j}\boldsymbol{b}_j^+\right]_{\substack{i=j_{start}\cdots j_{end}\\ j=j_{start}\cdots j_{end}}} \boldsymbol{q}^+(t) \tag{2}$$

with the Kronecker delta $\delta_{i,j}$. The favorable decoupled structure of (2) is lost as the expression of the radiative heat exchange

$$\boldsymbol{q}^{\mp}(t) = \boldsymbol{P}_z^{\mp}(t)\left(\boldsymbol{T}_z^{\mp}(t)\right)^4 + \boldsymbol{P}_s^{\mp}(t)\left(\boldsymbol{M}^{\mp}\boldsymbol{X}(t)\right)^4 \tag{3}$$

(cf. [35]) is considered, as shown on the left-hand side of Figure 2. The 4th power, emerging from the Stefan-Boltzmann law [37–39], is applied to each component of the respective vector. The $N_s \times 3N_s$ sparse matrix $\boldsymbol{M}^{\mp} = [\delta_{i,j}[1 \ \mp 1 \ {}^2\!/_3]]_{i=1\ldots N_s, j=1\ldots N_s}$ maps $\boldsymbol{X}(t)$ to the vector of bottom and top slab surface temperatures, respectively. Equ. (3) is a result of the net radiation method [37–40]. Remarks on the mapping matrixes $\boldsymbol{P}_z^{\mp}$ and $\boldsymbol{P}_s^{\mp}$ are provided in Appendix A.

In the considered furnace, only $N_{zc}^{\mp} = 4$ zones, i.e., the zones 2 through $N_z^{\mp} = 5$, are equipped with burners. They are referred to as *controllable* zones, and their temperatures are summarized in the vector $\boldsymbol{T}_{zc}^{\mp} = [T_{z,2}^{\mp}, \ldots, T_{z,N_z^{\mp}}^{\mp}]^{\mathsf{T}}$. Since zone 1 is not controllable, the empirical formula

$$(T_{z,2}^{\mp}(t))^4 - (T_{z,1}^{\mp}(t))^4 = T_{z,12}^{\Delta_z \mp} \tag{4}$$

with a constant value $T_{z,12}^{\Delta_z \mp}$ (unit K^4) is used to predict the unknown temperature $T_{z,1}^{\mp}$.

The *continuous-time* model (2) and (3) may assist in theoretical analyzes and will be used for formulating constraints and control objectives in Appendix B. For computer implementation, however, a reliably converging and accurate *discrete-time* representation is needed, as outlined in the following.

2.3. Discrete-time model

To obtain a discrete-time model, (3) can be evaluated at sampling points t_k ($k \in \mathbb{N}$), which must be set at least at event times $t_l^s \ \forall \ l \in \mathbb{N}$. Let $\boldsymbol{x}_{j,k}$ be the discrete-time approximation of $\boldsymbol{x}_j(t)$ at $t = t_k$. By assuming that the heat flux densities $q_j^{\mp}(t)$ are piecewise linear signals which may be discontinuous at t_k, i.e.,

$$q_j^{\mp}(t) = q_{j,k}^{1\mp}\frac{t_{k+1} - t}{\Delta t_k} + q_{j,k}^{2\mp}\frac{t - t_k}{\Delta t_k} \qquad \text{for} \qquad t_k \le t < t_{k+1},$$

Post-print version of the article: A. Steinboeck, K. Graichen, D. Wild, T. Kiefer, and A. Kugi, "Model-based trajectory planning, optimization, and open-loop control of a continuous slab reheating furnace", *Journal of Process Control*, vol. 21, no. 2, pp. 279–292, 2011. DOI: 10.1016/j.jprocont.2010.08.004

the discrete-time dynamic model of a single slab follows as (cf. [35])

$$\boldsymbol{x}_{j,k+1} = \boldsymbol{a}_{j,k}\boldsymbol{x}_{j,k} + \boldsymbol{b}^{1-}_{j,k}q^{1-}_{j,k} + \boldsymbol{b}^{1+}_{j,k}q^{1+}_{j,k} + \boldsymbol{b}^{2-}_{j,k}q^{2-}_{j,k} + \boldsymbol{b}^{2+}_{j,k}q^{2+}_{j,k} \tag{5a}$$

with

$$\boldsymbol{a}_{j,k} = \exp\left\{-\frac{12\bar{\lambda}_j(\boldsymbol{x}_{j,k})\Delta t_k}{\rho_j\bar{c}_j(\boldsymbol{x}_{j,k})D_j^2}\operatorname{diag}\left\{0 \quad 1 \quad 5\right\}\right\} \tag{5b}$$

$$\boldsymbol{b}^{1\mp}_{j,k} = \begin{bmatrix} \frac{\Delta t_k}{2\rho_j\bar{c}_j(\boldsymbol{x}_{j,k})D_j} \\ \mp\frac{D_j}{4\bar{\lambda}_j(\boldsymbol{x}_{j,k})}\left(-1+\left(1+\frac{\rho_j\bar{c}_j(\boldsymbol{x}_{j,k})D_j^2}{12\bar{\lambda}_j(\boldsymbol{x}_{j,k})\Delta t_k}\right)\left(1-\exp\left\{-\frac{12\bar{\lambda}_j(\boldsymbol{x}_{j,k})\Delta t_k}{\rho_j\bar{c}_j(\boldsymbol{x}_{j,k})D_j^2}\right\}\right)\right) \\ \frac{D_j}{8\bar{\lambda}_j(\boldsymbol{x}_{j,k})}\left(-1+\left(1+\frac{\rho_j\bar{c}_j(\boldsymbol{x}_{j,k})D_j^2}{60\bar{\lambda}_j(\boldsymbol{x}_{j,k})\Delta t_k}\right)\left(1-\exp\left\{-\frac{60\bar{\lambda}_j(\boldsymbol{x}_{j,k})\Delta t_k}{\rho_j\bar{c}_j(\boldsymbol{x}_{j,k})D_j^2}\right\}\right)\right) \end{bmatrix} \tag{5c}$$

$$\boldsymbol{b}^{2\mp}_{j,k} = \begin{bmatrix} \frac{\Delta t_k}{2\rho_j\bar{c}_j(\boldsymbol{x}_{j,k})D_j} \\ \mp\frac{D_j}{4\bar{\lambda}_j(\boldsymbol{x}_{j,k})}\left(1-\frac{\rho_j\bar{c}_j(\boldsymbol{x}_{j,k})D_j^2}{12\bar{\lambda}_j(\boldsymbol{x}_{j,k})\Delta t_k}\left(1-\exp\left\{-\frac{12\bar{\lambda}_j(\boldsymbol{x}_{j,k})\Delta t_k}{\rho_j\bar{c}_j(\boldsymbol{x}_{j,k})D_j^2}\right\}\right)\right) \\ \frac{D_j}{8\bar{\lambda}_j(\boldsymbol{x}_{j,k})}\left(1-\frac{\rho_j\bar{c}_j(\boldsymbol{x}_{j,k})D_j^2}{60\bar{\lambda}_j(\boldsymbol{x}_{j,k})\Delta t_k}\left(1-\exp\left\{-\frac{60\bar{\lambda}_j(\boldsymbol{x}_{j,k})\Delta t_k}{\rho_j\bar{c}_j(\boldsymbol{x}_{j,k})D_j^2}\right\}\right)\right) \end{bmatrix}, \tag{5d}$$

and the not necessarily constant sampling period $\Delta t_k = t_{k+1} - t_k$. By analogy to (2), (5) can be assembled for the whole system as (cf. [35])

$$\boldsymbol{X}_{k+1} = \boldsymbol{A}_k\boldsymbol{X}_k + \boldsymbol{B}^{1-}_k\boldsymbol{q}^{1-}_k + \boldsymbol{B}^{1+}_k\boldsymbol{q}^{1+}_k + \boldsymbol{B}^{2-}_k\boldsymbol{q}^{2-}_k + \boldsymbol{B}^{2+}_k\boldsymbol{q}^{2+}_k \tag{6a}$$

with $\boldsymbol{X}_k = [\boldsymbol{x}^\mathsf{T}_{j_{start},k}, \boldsymbol{x}^\mathsf{T}_{j_{start}+1,k}, \dots, \boldsymbol{x}^\mathsf{T}_{j_{end},k}]^\mathsf{T}$, $\boldsymbol{q}^{\alpha\mp}_k = [q^{\alpha\mp}_{j_{start},k}, q^{\alpha\mp}_{j_{start}+1,k}, \dots, q^{\alpha\mp}_{j_{end},k}]^\mathsf{T}$ $\forall\, \alpha \in \{1,2\}$, and the sparse matrices

$$\boldsymbol{A}_k = \left[\delta_{i,j}\boldsymbol{a}_{j,k}\right]_{i=j_{start}\cdots j_{end}, j=j_{start}\cdots j_{end}}, \qquad \boldsymbol{B}^{\alpha\mp}_k = \left[\delta_{i,j}\boldsymbol{b}^{\alpha\mp}_{j,k}\right]_{i=j_{start}\cdots j_{end}, j=j_{start}\cdots j_{end}} \quad \forall\, \alpha \in \{1,2\}. \tag{6b}$$

Together with (3), (6) constitutes an implicit, nonlinear equation for $\boldsymbol{X}_{k+1}$ requiring that $\boldsymbol{X}_k$, $\boldsymbol{T}^{\mp}_{z,k} = \boldsymbol{T}^{\mp}_z(t_k)$, and $\boldsymbol{T}^{\mp}_{z,k+1} = \boldsymbol{T}^{\mp}_z(t_{k+1})$ are known. The discrete-time model is used for designing required heat inputs into each slab (Subsection 4.2), for selecting optimal zone temperatures in controllable zones (Subsection 4.3), and for trajectory planning (Subsections 4.2 through 4.5).

3. Outline of the hierarchical control system

The primary *physical* inputs of the furnace system are the flow rates of fuel and combustion air. Directly controlling or optimizing them would require a sophisticated, mathematically complex model. Alternatively, the simple model outlined in the previous section is used in a *hierarchical control scheme*, which splits the control task into supervisory plant control, high-level furnace control, and low-level furnace zone temperature control.

3.1. Supervisory plant control

The task of supervisory plant control is to coordinate all rolling mill components, including the slab furnaces. The supervisory controller provides the so-called *slab schedule* which defines the sequence of slabs, the movement of slabs, some bounds on the slab reheating trajectories (cf. Subsection B.2.2), and the parameters listed in Table 1.

Post-print version of the article: A. Steinboeck, K. Graichen, D. Wild, T. Kiefer, and A. Kugi, "Model-based trajectory planning, optimization, and open-loop control of a continuous slab reheating furnace", *Journal of Process Control*, vol. 21, no. 2, pp. 279–292, 2011. DOI: 10.1016/j.jprocont.2010.08.004

Variables	Description
$t_{j,0}$	Time when slab enters the furnace
$t_{j,exit}$	Time when slab is withdrawn from the furnace
$T_{j,0}(y)$	Temperature profile at $t_{j,0}$
$\tilde{T}_{j,end}$	Desired temperature at $t_{j,exit}$ (homogeneous profile)
c_j, λ_j	Specific heat capacity and thermal conductivity (temperature-dependent)
D_j, W_j	Thickness and width of the slab
w_j	Weighting factor reflecting the monetary value of the slab

Table 1: Some parameters of the slab j specified by supervisory plant control.

A path-time diagram for each slab (cf. Figure 6c)) can be derived based on $t_{j,0}$, $t_{j,exit}$, and W_j of all considered slabs. The slab schedule is defined for a sufficiently large future period such that the high-level furnace controller, which is assumed to have *no* influence on the slab schedule (including the slab movements), can preplan future control actions.

3.2. High-level furnace control

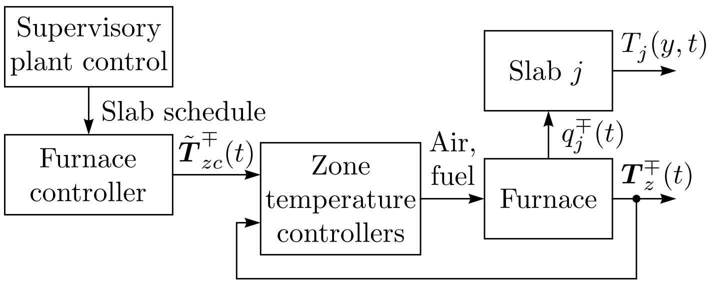

Figure 3: Hierarchical open-loop control system of a slab reheating furnace.

This paper focuses on high-level furnace control, which is referred to as *trajectory planning*. Its purpose is to provide low-level controllers with (optimal) reference signals $\tilde{\boldsymbol{T}}^{\mp}_{zc}(t)$ for controllable zone temperatures $\boldsymbol{T}^{\mp}_{zc}(t)$ based on a given slab schedule. To accomplish this task, a feedforward control scheme, as outlined in Figure 3, is developed in the following. Note that open-loop control is suitable for stable systems only. Weak additional conditions ensure that the system considered here belongs to this class. In [35], Lyapunov's theory is used to prove stability.

3.3. Low-level furnace zone temperature control

The inner feedback loop (low-level control) controls the temperatures $\boldsymbol{T}^{\mp}_{zc}(t)$ in the controllable furnace zones. It defines the flow rates of fuel and combustion air by means of standard PI controllers. Since the temperatures $\boldsymbol{T}^{\mp}_{zc}(t)$ can be measured by thermocouples, they are appropriate to link variables from high- and low-level control.

As usual for hierarchical or cascaded control structures, the design of the high-level controller assumes $\boldsymbol{T}^{\mp}_{zc}(t) = \tilde{\boldsymbol{T}}^{\mp}_{zc}(t)$. Two noteworthy problems are associated with this assumption: First, the slabs, of course, have an influence on the furnace temperatures, which is considered to be compensated by the low-level controllers. The second problem arises from restrictions on the fuel supply rates and is discussed in Subsection B.1.

Post-print version of the article: A. Steinboeck, K. Graichen, D. Wild, T. Kiefer, and A. Kugi, "Model-based trajectory planning, optimization, and open-loop control of a continuous slab reheating furnace", *Journal of Process Control*, vol. 21, no. 2, pp. 279–292, 2011. DOI: 10.1016/j.jprocont.2010.08.004

4. Trajectory planning and optimization

This section outlines a simple iterative trajectory planning and optimization algorithm used for high-level furnace control in order to compute optimal reference signals $\tilde{\boldsymbol{T}}^{\mp}_{zc}(t)$ for the period $[t_{k_0}, t_{k_1}]$. The approach is based on the *discrete-time* model (5) and (6) supplemented by (3). A nonlinear optimization problem is solved for designing $\tilde{\boldsymbol{T}}^{\mp}_{zc,k} = \tilde{\boldsymbol{T}}^{\mp}_{zc}(t_k)$. However, even if only a finite period $[t_{k_0}, t_{k_1}]$ is considered, the optimization problem exhibits $(N^-_{zc} + N^+_{zc})(k_1 - k_0 + 1)$ degrees of freedom. To circumvent such high-dimensional optimization problems, an *iterative two-step approach* is proposed in the following. Figure 4 outlines a scheme of the iterative method.

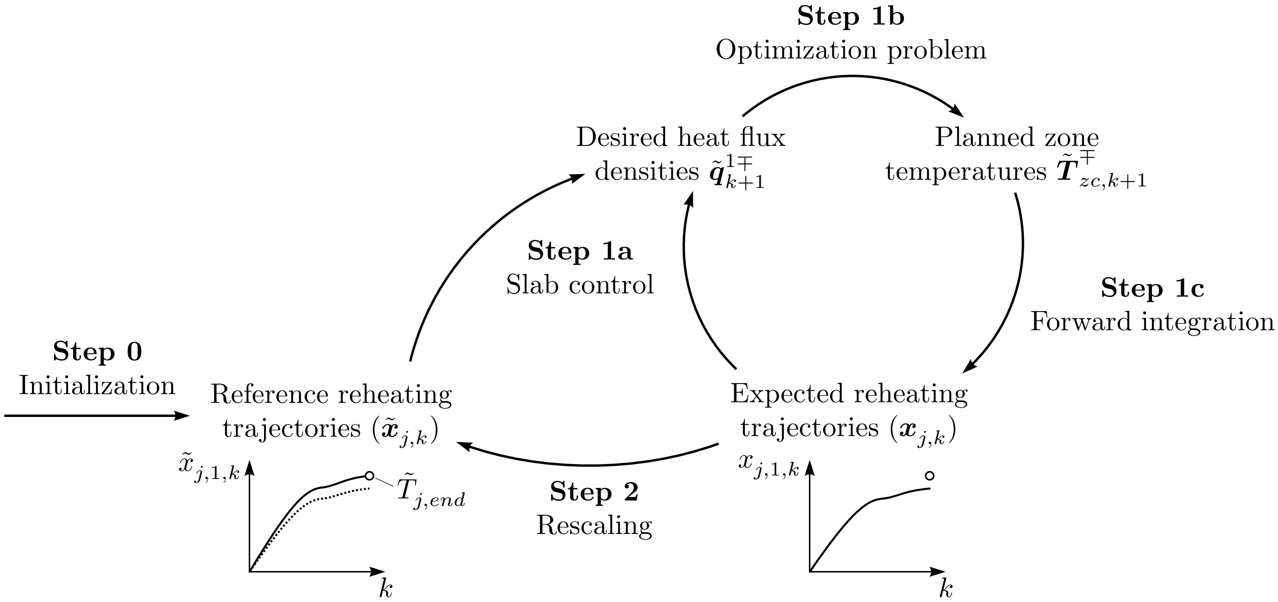

Figure 4: Iterative trajectory planning and optimization.

First, an initial guess of so-called *reference reheating trajectories* $(\tilde{\boldsymbol{x}}_{j,k})$ has to be made for all considered slabs (step 0). The next step is divided into three substeps 1a, 1b, and 1c, which are successively executed for each sampling point t_k within the planning period $[t_{k_0}, t_{k_1}]$, i. e., the values at t_{k+1} are to be planned given that the planned values at t_k are known. In step 1a, the dynamic subsystems (5) of the slabs $j \in J$ are considered, and *desired* heat flux densities $\tilde{\boldsymbol{q}}^{1\mp}_{k+1}$ are determined which ensure that the slab states follow some reference trajectories $(\tilde{\boldsymbol{x}}_{j,k})$ ending at the desired final state $\tilde{\boldsymbol{x}}_{j,end} = [\tilde{T}_{j,end}, 0, 0]^{\mathsf{T}}$. Within step 1b, the bottom and the top half of the furnace are individually considered, and the reference values $\tilde{\boldsymbol{T}}^{\mp}_{zc,k+1}$ are chosen such that the difference between $\boldsymbol{q}^{1\mp}_{k+1}$ and $\tilde{\boldsymbol{q}}^{1\mp}_{k+1}$ is minimized. In step 1c, the states $\boldsymbol{X}_{k+1}$ are computed with the planned input values $\tilde{\boldsymbol{T}}^{\mp}_{zc,k+1}$.

In the second step, the trajectories $(\boldsymbol{x}_{j,k})$ obtained in step 1 are rescaled such that the desired final states $\tilde{\boldsymbol{x}}_{j,end}$ are exactly reached. The rescaled trajectories $(\boldsymbol{x}_{j,k})$ are used as new reference trajectories $(\tilde{\boldsymbol{x}}_{j,k})$, and the iterative process may be restarted at step 1a. Depending on the initial guess of $(\tilde{\boldsymbol{x}}_{j,k})$, usually one or two executions of the overall iteration loop suffice. Finally, the planned zone temperature trajectories $(\tilde{\boldsymbol{T}}^{\mp}_{zc,k})$ are commanded to the low-level controllers.

In the following, the steps of the iterative method are individually explained. Although, the discussion of the steps 0 and 1a are confined to a *single* slab j, they have to be carried out (individually) for all slabs.

4.1. Step 0 - Initialization

An initial reference trajectory $(\tilde{\boldsymbol{x}}_{j,k})$ is designed based on parameters listed in Table 2. Later, it will be replaced by a more realistic, optimized trajectory. The shape of the initial guess was 'heuristically' derived from measurements in the real furnace.

Post-print version of the article: A. Steinboeck, K. Graichen, D. Wild, T. Kiefer, and A. Kugi, "Model-based trajectory planning, optimization, and open-loop control of a continuous slab reheating furnace", *Journal of Process Control*, vol. 21, no. 2, pp. 279–292, 2011. DOI: 10.1016/j.jprocont.2010.08.004

Variables	Description
$t_{j,0}$, $t_{j,exit}$, $T_{j,0}(y)$, $\tilde{T}_{j,end}$	See Table 1
$t_{j,homo}$	Minimum length of the homogenization period
$\delta_{j,homo} \in [0,1]$	Fraction of temperature change that is left for the homogenization period
γ_j	Normalized smoothing radius for the transition between the main heating period and the homogenization period

Table 2: Parameters specifying the initial reference trajectory of the slab j, see also Figure 5.

The values of $t_{j,0}$, $t_{j,exit}$, $T_{j,0}(y)$, $\tilde{T}_{j,end}$, and $t_{j,homo}$ are governed by the supervisory plant controller. Let

$$\tau_j(t) = \begin{cases} 0 & \text{if } t \le t_{j,0} \\ \frac{t - t_{j,0}}{t_{j,exit} - t_{j,0}} & \text{if } t_{j,0} < t \le t_{j,exit} \\ 1 & \text{else} \end{cases} \tag{7}$$

be a normalized time variable. Then, a continuous shape function $\theta_j(\tau_j) : [0,1] \to [0,1]$ with $\theta_j(0) = 0$ and $\theta_j(1) = 1$ is utilized to construct the initial reference trajectory as $\tilde{T}_j(y,t) = (1 - \theta_j(\tau_j(t)))T_{j,0}(y) + \theta_j(\tau_j(t))\tilde{T}_{j,end}(y)$, or approximated in terms of Galerkin coefficients of the discrete-time system as $\tilde{\boldsymbol{x}}_{j,k} = (1 - \theta_j(\tau_j(t_k)))\boldsymbol{x}_{j,0} + \theta_j(\tau_j(t_k))\tilde{\boldsymbol{x}}_{j,end}$.

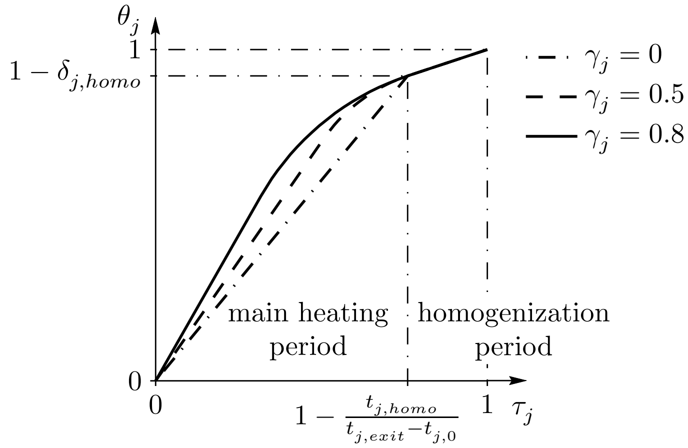

Figure 5: Normalized shape of the initial reference trajectory.

The shapes $\theta_j(\tau_j)$ shown in Figure 5 proved suitable in the practical application. They are controlled by the parameters $\delta_{j,homo}$ and γ_j and consist of two linear sections joined by a circular arc (radius γ_j). In the first period of the reheating process (main heating period), the slope of $\theta_j(\tau_j)$ is relatively large. Therefore, the slab is rapidly heated and its surface temperatures will significantly exceed its core temperature. Aiming for a homogeneous final temperature profile, the slope of $\theta_j(\tau_j)$ is reduced during the second period, referred to as homogenization period. A smooth transition between the two linear sections of $\theta_j(\tau_j)$ is achieved by the circular arc that terminates the main heating period. The influence of the arc radius γ_j is indicated in Figure 5.

A fraction $\delta_{j,homo}$ of the desired total temperature change $\tilde{T}_{j,end} - T_{j,0}(y)$ is allocated to the homogenization period. The two parameters $\delta_{j,homo}$ and γ_j are chosen by the algorithm depending on the constraints of the slab temperature trajectory (cf. Subsection B.2.2). Usually, $0 < \delta_{j,homo} \ll 1$ is a good choice, which ensures that $\theta_j(\tau_j)$ is monotonically increasing.

Post-print version of the article: A. Steinboeck, K. Graichen, D. Wild, T. Kiefer, and A. Kugi, "Model-based trajectory planning, optimization, and open-loop control of a continuous slab reheating furnace", *Journal of Process Control*, vol. 21, no. 2, pp. 279–292, 2011. DOI: 10.1016/j.jprocont.2010.08.004
The content of this post-print version is identical to the published paper but without the publisher's final layout or copy editing.

4.2. Step 1a - Slab control

Given the reference trajectory $(\tilde{\boldsymbol{x}}_{j,k})$, the *desired* heat inputs $(\tilde{q}^{1\mp}_{j,k})$ and $(\tilde{q}^{2\mp}_{j,k})$ can be planned. At first glance, the discrete-time system (5) seems to have four independent inputs $q^{1-}_{j,k}$, $q^{1+}_{j,k}$, $q^{2-}_{j,k}$, and $q^{2+}_{j,k}$. However, $q^{1\mp}_{j,k+1}$ implicitly depends on $q^{2\mp}_{j,k}$, which imposes some restrictions on the planning process. Unfortunately, this dependence cannot be formulated without considering the whole furnace system (3) and (6).

If the slabs do not change their position at t_{k+1}, the continuity of temperatures in (3) ensures $q^{1\mp}_{j,k+1} = q^{2\mp}_{j,k}$. Even if slabs are moved, $q^{1\mp}_{j,k+1} - q^{2\mp}_{j,k}$ remains small such that

$$q^{1\mp}_{j,k+1} = q^{2\mp}_{j,k} \tag{8}$$

is a justifiable assumption for planning $(\tilde{q}^{1\mp}_{j,k})$ and $(\tilde{q}^{2\mp}_{j,k})$.

The task of designing $(\tilde{q}^{1\mp}_{j,k})$ for some given $(\tilde{\boldsymbol{x}}_{j,k})$ essentially requires an inversion of the system (5). Since there are less independent inputs than system states, planning the series $(\tilde{q}^{1\mp}_{j,k})$ such that $(q^{1\mp}_{j,k}) = (\tilde{q}^{1\mp}_{j,k}) \Rightarrow (\boldsymbol{x}_{j,k}) = (\tilde{\boldsymbol{x}}_{j,k})$ is generally not feasible. However, a good match between $(\boldsymbol{x}_{j,k})$ and $(\tilde{\boldsymbol{x}}_{j,k})$ should suffice.

Simple *proportional* SISO feedback control laws are applied to the simulation model (5) for planning $(\tilde{q}^{1\mp}_{j,k})$. They generate input signals of reasonable amplitudes, can easily cope with the time-variant character of the system, and are robust against boundedness of inputs.

By means of (8) and the input transformation

$$\begin{bmatrix} q^{\Sigma}_{j,k} \\ q^{\Delta}_{j,k} \end{bmatrix} = \begin{bmatrix} 1 & 1 \\ -1 & 1 \end{bmatrix} \begin{bmatrix} q^{1-}_{j,k} \\ q^{1+}_{j,k} \end{bmatrix}, \tag{9}$$

(5) disintegrates into a 2nd order system

$$\begin{bmatrix} x_{j,1,k+1} \\ x_{j,3,k+1} \end{bmatrix} = \boldsymbol{a}^{\Sigma}_{j,k} \begin{bmatrix} x_{j,1,k} \\ x_{j,3,k} \end{bmatrix} + \boldsymbol{b}^{\Sigma 1}_{j,k} q^{\Sigma}_{j,k} + \boldsymbol{b}^{\Sigma 2}_{j,k} q^{\Sigma}_{j,k+1} \tag{10a}$$

$$\boldsymbol{a}^{\Sigma}_{j,k} = \operatorname{diag}\left\{ 1 \quad \exp\left\{ -\frac{60\bar{\lambda}_j(\boldsymbol{x}_{j,k})\Delta t_k}{\rho_j \bar{c}_j(\boldsymbol{x}_{j,k}) D_j^2} \right\} \right\} \tag{10b}$$

$$\boldsymbol{b}^{\Sigma 1}_{j,k} = \left[\frac{\Delta t_k}{2\rho_j \bar{c}_j(\boldsymbol{x}_{j,k}) D_j} \quad \frac{D_j}{8\bar{\lambda}_j(\boldsymbol{x}_{j,k})} \left(-1 + \left(1 + \frac{\rho_j \bar{c}_j(\boldsymbol{x}_{j,k}) D_j^2}{60\bar{\lambda}_j(\boldsymbol{x}_{j,k})\Delta t_k} \right) \left(1 - \exp\left\{ -\frac{60\bar{\lambda}_j(\boldsymbol{x}_{j,k})\Delta t_k}{\rho_j \bar{c}_j(\boldsymbol{x}_{j,k}) D_j^2} \right\} \right) \right) \right]^{\mathsf{T}} \tag{10c}$$

$$\boldsymbol{b}^{\Sigma 2}_{j,k} = \left[\frac{\Delta t_k}{2\rho_j \bar{c}_j(\boldsymbol{x}_{j,k}) D_j} \quad \frac{D_j}{8\bar{\lambda}_j(\boldsymbol{x}_{j,k})} \left(1 - \frac{\rho_j \bar{c}_j(\boldsymbol{x}_{j,k}) D_j^2}{60\bar{\lambda}_j(\boldsymbol{x}_{j,k})\Delta t_k} \left(1 - \exp\left\{ -\frac{60\bar{\lambda}_j(\boldsymbol{x}_{j,k})\Delta t_k}{\rho_j \bar{c}_j(\boldsymbol{x}_{j,k}) D_j^2} \right\} \right) \right) \right]^{\mathsf{T}} \tag{10d}$$

and a 1st order system

$$x_{j,2,k+1} = a^{\Delta}_{j,k} x_{j,2,k} + b^{\Delta 1}_{j,k} q^{\Delta}_{j,k} + b^{\Delta 2}_{j,k} q^{\Delta}_{j,k+1} \tag{11a}$$

$$a^{\Delta}_{j,k} = \exp\left\{ -\frac{12\bar{\lambda}_j(\boldsymbol{x}_{j,k})\Delta t_k}{\rho_j \bar{c}_j(\boldsymbol{x}_{j,k}) D_j^2} \right\} \tag{11b}$$

$$b^{\Delta 1}_{j,k} = \frac{D_j}{4\bar{\lambda}_j(\boldsymbol{x}_{j,k})} \left(-1 + \left(1 + \frac{\rho_j \bar{c}_j(\boldsymbol{x}_{j,k}) D_j^2}{12\bar{\lambda}_j(\boldsymbol{x}_{j,k})\Delta t_k} \right) \left(1 - \exp\left\{ -\frac{12\bar{\lambda}_j(\boldsymbol{x}_{j,k})\Delta t_k}{\rho_j \bar{c}_j(\boldsymbol{x}_{j,k}) D_j^2} \right\} \right) \right) \tag{11c}$$

$$b^{\Delta 2}_{j,k} = \frac{D_j}{4\bar{\lambda}_j(\boldsymbol{x}_{j,k})} \left(1 - \frac{\rho_j \bar{c}_j(\boldsymbol{x}_{j,k}) D_j^2}{12\bar{\lambda}_j(\boldsymbol{x}_{j,k})\Delta t_k} \left(1 - \exp\left\{ -\frac{12\bar{\lambda}_j(\boldsymbol{x}_{j,k})\Delta t_k}{\rho_j \bar{c}_j(\boldsymbol{x}_{j,k}) D_j^2} \right\} \right) \right). \tag{11d}$$

Introducing the error variables

$$e^{\Sigma}_{j,k} = x_{j,1,k} - \begin{bmatrix} 1 & 0 & 0 \end{bmatrix} \tilde{\boldsymbol{x}}_{j,k}, \qquad e^{\Delta}_{j,k} = x_{j,2,k} - \begin{bmatrix} 0 & 1 & 0 \end{bmatrix} \tilde{\boldsymbol{x}}_{j,k} \tag{12a}$$

and the proportional SISO feedback laws

$$\tilde{q}^{\Sigma}_{j,k+1} = -k^{\Sigma}_{j,k} e^{\Sigma}_{j,k}, \qquad \tilde{q}^{\Delta}_{j,k+1} = -k^{\Delta}_{j,k} e^{\Delta}_{j,k} \tag{12b}$$

allows exponential stabilization of *all* states of the systems (10) and (11)—and therefore of the system (5)—

Post-print version of the article: A. Steinboeck, K. Graichen, D. Wild, T. Kiefer, and A. Kugi, "Model-based trajectory planning, optimization, and open-loop control of a continuous slab reheating furnace", *Journal of Process Control*, vol. 21, no. 2, pp. 279–292, 2011. DOI: 10.1016/j.jprocont.2010.08.004
The content of this post-print version is identical to the published paper but without the publisher's final layout or copy editing.

at any homogeneous temperature profile. The stability proof is based on the induced norm of the transition matrix describing the error dynamics of the closed-loop system (autonomous system), which has a triangular structure. Based on this, it can be shown that the infinity norms of both $[{e^{\Sigma}_{j,k+1}}^{\mathsf{T}}, {e^{\Sigma}_{j,k}}^{\mathsf{T}}]$ and $[{e^{\Delta}_{j,k+1}}^{\mathsf{T}}, {e^{\Delta}_{j,k}}^{\mathsf{T}}]$ decrease exponentially. The time indices in (12b) ($k+1$ on the left-hand side and k on the right-hand side) are in line with the planning approach of step 1, since the control variables at t_{k+1} are planned given that the planned values at t_k are known (cf. the discussion at the beginning of Section 4).

In (12a), the current state $\boldsymbol{x}_{j,k}$ is either the initial state $\boldsymbol{x}_{j,0}$ (slabs that have just entered the furnace) or an estimate previously computed in step 1c (cf. Subsection 4.4). The feedback laws (12b) allow individual control of $x_{j,1,k}$ (mean slab temperature) and $x_{j,2,k}$ (asymmetry of the temperature profile).

The conditions $k^{\Sigma}_{j,k} > 0$ and $k^{\Delta}_{j,k} > 0$ are necessary for exponential stability. Moreover, upper limits for the sampling period Δt_k, the controller gains $k^{\Sigma}_{j,k}$ and $k^{\Delta}_{j,k}$ and limitations concerning their time dependence can be readily derived from the stability proof. In practical terms, even for the discrete-time control laws (12), the upper limits of $k^{\Sigma}_{j,k}$ and $k^{\Delta}_{j,k}$ do not correspond to the stability bound but to constraints on the heat inputs $q^{1\mp}_{j,k+1}$. Fortunately, the proposed controllers are sufficiently robust against limitations of the inputs $q^{1\mp}_{j,k+1}$, which may be interpreted as a *reduction* of $k^{\Sigma}_{j,k}$ or $k^{\Delta}_{j,k}$ or both.

By finally applying the inverse of the transformation (9) to (12), the planning formula for the original inputs of (5) is found as

$$\begin{bmatrix} \tilde{q}^{1-}_{j,k+1} \\ \tilde{q}^{1+}_{j,k+1} \end{bmatrix} = \frac{1}{2} \begin{bmatrix} -k^{\Sigma}_{j,k} & k^{\Delta}_{j,k} & 0 \\ -k^{\Sigma}_{j,k} & -k^{\Delta}_{j,k} & 0 \end{bmatrix} (\boldsymbol{x}_{j,k} - \tilde{\boldsymbol{x}}_{j,k}).$$

4.3. Step 1b - Optimization problem

Now, since the desired inputs $\tilde{q}^{1\mp}_{j,k+1}$ are known for each slab $j \in J$, it remains to find temperatures $\tilde{\boldsymbol{T}}^{\mp}_{zc,k+1}$ for the controllable zones which best realize the desired values $\tilde{\boldsymbol{q}}^{1\mp}_{k+1} = [\tilde{q}^{\mp}_{j_{start},k+1}, \tilde{q}^{\mp}_{j_{start}+1,k+1}, \ldots, \tilde{q}^{\mp}_{j_{end},k+1}]^{\mathsf{T}}$. The model (3) and (6) allows individual consideration of the bottom and the top half of the furnace. Therefore, this subsection solves the static optimization problem of achieving N_s control objectives for $\boldsymbol{q}^{1\mp}_{k+1}$ by choosing only $N^{\mp}_z$ setpoint values $\tilde{\boldsymbol{T}}^{\mp}_{z,k+1}$. At first sight, it may seem inconsistent that the control problem is solved for $\tilde{\boldsymbol{T}}^{\mp}_{z,k+1}$ rather than $\tilde{\boldsymbol{T}}^{\mp}_{zc,k+1}$, although $T^{\mp}_{z,1,k+1}$ is generally *not* individually controllable (cf. Section 2.2). However, the approach further simplifies the mathematical expressions, and the empirical constraint (4) can still be approximately accounted for. If restrictions on $\tilde{\boldsymbol{T}}^{\mp}_{z,k+1}$ (cf. (20)) are active, the number of controllable inputs is reduced, at least temporarily.

4.3.1. Nonlinear optimization problem

Because of $N^{\mp}_z < N_s$, it is generally impossible to accomplish all control objectives exactly. A common method of resolving the dilemma are *optimization* problems ensuring that the control objectives are satisfied as *good* as possible. For instance, $\tilde{\boldsymbol{T}}^{\mp}_{z,k+1}$ can be chosen such that the cost function

$$(\boldsymbol{q}^{1\mp}_{k+1} - \tilde{\boldsymbol{q}}^{1\mp}_{k+1})^{\mathsf{T}} \boldsymbol{W}^{\mp}_{k+1} (\boldsymbol{q}^{1\mp}_{k+1} - \tilde{\boldsymbol{q}}^{1\mp}_{k+1}) \tag{13}$$

with some positive definite $\boldsymbol{W}^{\mp}_{k+1} \in \mathbb{R}^{N_s \times N_s}$ is minimized. Again the stipulation $\tilde{\boldsymbol{T}}^{\mp}_{z,k+1} = \boldsymbol{T}^{\mp}_{z,k+1}$ from Subsection 3.3 is used.

Evaluating (3) at t_{k+1} yields the expected values $\boldsymbol{q}^{1\mp}_{k+1}$. Unfortunately, (3) contains the unknown states $\boldsymbol{X}_{k+1}$ in a nonlinear fashion. To simplify the problem, the desired value $\boldsymbol{A}_k \boldsymbol{X}_k + \boldsymbol{B}^{1-}_k \boldsymbol{q}^{1-}_k + \boldsymbol{B}^{1+}_k \boldsymbol{q}^{1+}_k + \boldsymbol{B}^{2-}_k \tilde{\boldsymbol{q}}^{1-}_{k+1} + \boldsymbol{B}^{2+}_k \tilde{\boldsymbol{q}}^{1+}_{k+1}$ is substituted for $\boldsymbol{X}_{k+1}$ (cf. (6a)).

4.3.2. Constraints

The slab reheating process is restricted by constraints on both input signals and system states. The constraints are discussed in Appendix B. The most important results are summarized in the following.

Post-print version of the article: A. Steinboeck, K. Graichen, D. Wild, T. Kiefer, and A. Kugi, "Model-based trajectory planning, optimization, and open-loop control of a continuous slab reheating furnace", *Journal of Process Control*, vol. 21, no. 2, pp. 279–292, 2011. DOI: 10.1016/j.jprocont.2010.08.004
The content of this post-print version is identical to the published paper but without the publisher's final layout or copy editing.

The preplanned reference signals must satisfy the temperature constraints (20), i. e.,

$$T^{\mp}_{z,i,min}(t) \le \tilde{T}^{\mp}_{z,i}(t) \le T^{\mp}_{z,i,max}(t), \quad \dot{T}^{\mp}_{z,i,min}(t) \le \dot{\tilde{T}}^{\mp}_{z,i}(t) \le \dot{T}^{\mp}_{z,i,max}(t) \quad \forall\, i \in \{1,2,\ldots,N^{\mp}_z\}. \tag{14}$$

It is assumed that *any* reference trajectory $\tilde{\boldsymbol{T}}^{\mp}_z(t)$ satisfying (14) (and (4)) can be realized by the furnace system, which is a prerequisite for the hierarchical control structure. Consider that the planned values $\tilde{\boldsymbol{T}}^{\mp}_{z,k}$ are known. Then, (14) can be formulated in the discrete-time domain as

$$\begin{aligned}\underline{T}^{\mp}_{z,i,k+1} &= \max\{T^{\mp}_{z,i,min}(t_{k+1}), \tilde{T}^{\mp}_{z,i,k} + \Delta t_k \dot{T}^{\mp}_{z,i,min}(t_k)\} \le \tilde{T}^{\mp}_{z,i,k+1} \\ &\le \min\{T^{\mp}_{z,i,max}(t_{k+1}), \tilde{T}^{\mp}_{z,i,k} + \Delta t_k \dot{T}^{\mp}_{z,i,max}(t_k)\} = \overline{T}^{\mp}_{z,i,k+1} \qquad \forall\, i \in \{1,2,\ldots,N^{\mp}_z\}.\end{aligned}$$

As defined in Subsection B.2, the system states are restricted by soft constraints $\boldsymbol{x}_{j,k+1} \in X^S_j(t_{k+1})\ \forall\, j \in J$, $k \in \mathbb{N}$ and hard constraints $\boldsymbol{x}_{j,k+1} \in X^H_j\ \forall\, j \in J,\ k \in \mathbb{N}$. In contrast to the hard constraints, the time-dependent set $X^S_j(t) \subseteq X^H_j$ may be relaxed or abandoned if otherwise a solution of the planning problem is not feasible.

Consider for a single slab $j \in J$ that the *expected* state $\boldsymbol{x}_{j,k} \in X^S_j(t_k)$ and the previous heat inputs $q^{1\mp}_{j,k}$ are known. Then, (5) allows the computation of limits on $q^{2\mp}_{j,k} = q^{1\mp}_{j,k+1}$ which ensure that $\boldsymbol{x}_{j,k+1}$ remains within a certain set. Hence, soft constraints $\underline{q}^{S\mp}_{j,k+1}$, $\overline{q}^{S\mp}_{j,k+1}$ and hard constraints $\underline{q}^{H\mp}_{j,k+1}$, $\overline{q}^{H\mp}_{j,k+1}$ can be found such that

$$\underline{q}^{S-}_{j,k+1} \le q^{1-}_{j,k+1} \le \overline{q}^{S-}_{j,k+1} \ \wedge\ \underline{q}^{S+}_{j,k+1} \le q^{1+}_{j,k+1} \le \overline{q}^{S+}_{j,k+1} \quad \Leftrightarrow \quad \boldsymbol{x}_{j,k+1} \in X^S_j(t_{k+1}) \tag{15a}$$

$$\underline{q}^{H-}_{j,k+1} \le q^{1-}_{j,k+1} \le \overline{q}^{H-}_{j,k+1} \ \wedge\ \underline{q}^{H+}_{j,k+1} \le q^{1+}_{j,k+1} \le \overline{q}^{H+}_{j,k+1} \quad \Leftrightarrow \quad \boldsymbol{x}_{j,k+1} \in X^H_j \tag{15b}$$

are at least approximately satisfied. Clearly, these restrictions can be individually derived for all $j \in J$. To obtain henceforth a shorter notation, let $\underline{q}^{S\mp}_{j,k+1}$, $\overline{q}^{S\mp}_{j,k+1}$, $\underline{q}^{H\mp}_{j,k+1}$, and $\overline{q}^{H\mp}_{j,k+1}$ for $j \in J$, as well as $\underline{T}^{\mp}_{z,i,k+1}$ and $\overline{T}^{\mp}_{z,i,k+1}$ for $i \in \{1,2,\ldots,N^{\mp}_z\}$ be summarized in the vectors $\underline{\boldsymbol{q}}^{S\mp}_{k+1}$, $\overline{\boldsymbol{q}}^{S\mp}_{k+1}$, $\underline{\boldsymbol{q}}^{H\mp}_{k+1}$, $\overline{\boldsymbol{q}}^{H\mp}_{k+1}$, $\underline{\boldsymbol{T}}^{\mp}_{z,k+1}$, and $\overline{\boldsymbol{T}}^{\mp}_{z,k+1}$, respectively.

4.3.3. Reformulation as quadratic optimization problem

So far, both the cost function (13) and the constraints (15) are *nonlinear* with respect to the optimization variables $\tilde{\boldsymbol{T}}^{\mp}_{z,k+1}$. Fortunately, by virtue of (3), the optimization problem simplifies to a (standard) *quadratic program* with *linear* constraints if formulated in terms of $(\tilde{\boldsymbol{T}}^{\mp}_{z,k+1})^4$ rather than in terms of $\tilde{\boldsymbol{T}}^{\mp}_{z,k+1}$.

Using the monotonicity relation materialized in (3) and discussed in Appendix A, the lower-bound in (15a) is reformulated as

$$\underline{\boldsymbol{q}}^{S\mp}_{k+1} \le \boldsymbol{q}^{1\mp}_{k+1} = \boldsymbol{P}^{\mp}_z(t_k)(\boldsymbol{T}^{\mp}_{z,k+1})^4 + \boldsymbol{P}^{\mp}_s(t_k)(\boldsymbol{M}^{\mp}\boldsymbol{X}_{k+1})^4. \tag{16}$$

Here, $\underline{\boldsymbol{q}}^{S\mp}_{k+1} \le \boldsymbol{q}^{1\mp}_{k+1}$ means that the inequality relation holds true for all corresponding components of $\underline{\boldsymbol{q}}^{S\mp}_{k+1}$ and $\boldsymbol{q}^{1\mp}_{k+1}$. In (16), the unknown state $\boldsymbol{X}_{k+1}$ is replaced by the conservative approximation $\boldsymbol{A}_k\boldsymbol{X}_k + \boldsymbol{B}^{1-}_k\boldsymbol{q}^{1-}_k + \boldsymbol{B}^{1+}_k\boldsymbol{q}^{1+}_k + \boldsymbol{B}^{2-}_k\underline{\boldsymbol{q}}^{S-}_{k+1} + \boldsymbol{B}^{2+}_k\underline{\boldsymbol{q}}^{S+}_{k+1}$. The term *conservative* is justified because of (6a) and the remarks given in Appendix A. Other inequalities containing $\overline{\boldsymbol{q}}^{S\mp}_{k+1}$, $\underline{\boldsymbol{q}}^{H\mp}_{k+1}$, and $\overline{\boldsymbol{q}}^{H\mp}_{k+1}$ can be derived by analogy to (16). However, $\underline{\boldsymbol{q}}^{H\mp}_{k+1}$ and $\overline{\boldsymbol{q}}^{H\mp}_{k+1}$ are not required for the moment, because $X^S_j(t) \subseteq X^H_j$.

Undesirable fluctuations of the zone temperatures can be avoided by adding the term

$$\left((\tilde{\boldsymbol{T}}^{\mp}_{z,k+1})^4 - (\tilde{\boldsymbol{T}}^{\mp}_{z,k})^4\right)^{\mathsf{T}} \boldsymbol{W}^{\Delta_t\mp}_{k+1}\left((\tilde{\boldsymbol{T}}^{\mp}_{z,k+1})^4 - (\tilde{\boldsymbol{T}}^{\mp}_{z,k})^4\right) \tag{17a}$$

with positive semidefinite $\boldsymbol{W}^{\Delta_t\mp}_{k+1} \in \mathbb{R}^{N^{\mp}_z \times N^{\mp}_z}$ to the cost function (13). If the process operation strategy requires specific offsets between neighboring zone temperatures, the cost function can be extended by

$$\left(\boldsymbol{\Delta}^{\mp}_z(\tilde{\boldsymbol{T}}^{\mp}_{z,k+1})^4 - \boldsymbol{T}^{\Delta_z\mp}_z\right)^{\mathsf{T}} \boldsymbol{W}^{\Delta_z\mp}_{k+1}\left(\boldsymbol{\Delta}^{\mp}_z(\tilde{\boldsymbol{T}}^{\mp}_{z,k+1})^4 - \boldsymbol{T}^{\Delta_z\mp}_z\right) \tag{17b}$$

Post-print version of the article: A. Steinboeck, K. Graichen, D. Wild, T. Kiefer, and A. Kugi, "Model-based trajectory planning, optimization, and open-loop control of a continuous slab reheating furnace", *Journal of Process Control*, vol. 21, no. 2, pp. 279–292, 2011. DOI: 10.1016/j.jprocont.2010.08.004
The content of this post-print version is identical to the published paper but without the publisher's final layout or copy editing.

with $\boldsymbol{\Delta}_z^{\mp} = \left[\delta_{i,j} - \delta_{i,j-1}\right]_{i=1\ldots N_z^{\mp}-1, j=1\ldots N_z^{\mp}}$, a constant vector $\boldsymbol{T}_z^{\Delta_z \mp} \in \mathbb{R}^{N_z^{\mp}-1}$, and positive semidefinite $\boldsymbol{W}_{k+1}^{\Delta_z \mp} \in \mathbb{R}^{N_z^{\mp}-1 \times N_z^{\mp}-1}$. This is an appropriate method of implementing the empirical formula (4), i. e., of coupling $\tilde{T}_{z,1,k+1}^{\mp}$ with $\tilde{T}_{z,2,k+1}^{\mp}$. The corresponding coefficient in the main diagonal of $\boldsymbol{W}_{k+1}^{\Delta_z \mp}$ can get a large (penalty) value, which effectively reduces the degrees of freedom of the optimization problem by 1.

Adding up the cost functions (13) and (17) and using (3) yield the optimal zone temperature values as

$$
\begin{aligned}
&\tilde{\boldsymbol{T}}_{z,k+1}^{\mp} = \\
&\left(\underset{(\tilde{\boldsymbol{T}}_{z,k+1}^{\mp})^4 \in (\mathbb{R}^+)^{N_z^{\mp}}}{\arg\min} \left\{ \begin{array}{l} (\tilde{\boldsymbol{T}}_{z,k+1}^{\mp})^{4^{\mathsf{T}}} \big(\boldsymbol{P}_z^{\mp\mathsf{T}}(t_k) \boldsymbol{W}_{k+1}^{\mp} \boldsymbol{P}_z^{\mp}(t_k) + \boldsymbol{W}_{k+1}^{\Delta_t \mp} + \boldsymbol{\Delta}_z^{\mp\mathsf{T}} \boldsymbol{W}_{k+1}^{\Delta_z \mp} \boldsymbol{\Delta}_z^{\mp}\big) (\tilde{\boldsymbol{T}}_{z,k+1}^{\mp})^4 + \ldots \\ \ldots\ 2\, (\tilde{\boldsymbol{T}}_{z,k+1}^{\mp})^{4^{\mathsf{T}}} \Big(\boldsymbol{P}_z^{\mp\mathsf{T}}(t_k) \boldsymbol{W}_{k+1}^{\mp} \Big(\boldsymbol{P}_s^{\mp}(t_k) \big(\boldsymbol{M}^{\mp} \big(\boldsymbol{A}_k \boldsymbol{X}_k + \boldsymbol{B}_k^{1-} \boldsymbol{q}_k^{1-} + \boldsymbol{B}_k^{1+} \boldsymbol{q}_k^{1+} \ \ldots \\ \ldots + \boldsymbol{B}_k^{2-} \tilde{\boldsymbol{q}}_{k+1}^{1-} + \boldsymbol{B}_k^{2+} \tilde{\boldsymbol{q}}_{k+1}^{1+} \big)\big)^4 - \tilde{\boldsymbol{q}}_{k+1}^{1\mp} \Big) - \boldsymbol{W}_{k+1}^{\Delta_t \mp} (\tilde{\boldsymbol{T}}_{z,k}^{\mp})^4 - \boldsymbol{\Delta}_z^{\mp\mathsf{T}} \boldsymbol{W}_{k+1}^{\Delta_z \mp} \boldsymbol{T}_z^{\Delta_z \mp} \Big) \end{array} \right\} \right) \\
&\qquad \boldsymbol{P}_z^{\mp}(t_k) (\tilde{\boldsymbol{T}}_{z,k+1}^{\mp})^4 \ \geq\ \underline{\boldsymbol{q}}_{k+1}^{S\mp} - \boldsymbol{P}_s^{\mp}(t_k) \big(\boldsymbol{M}^{\mp} \big(\boldsymbol{A}_k \boldsymbol{X}_k + \ldots \\
&\qquad\qquad \ldots\ \boldsymbol{B}_k^{1-} \boldsymbol{q}_k^{1-} + \boldsymbol{B}_k^{1+} \boldsymbol{q}_k^{1+} + \boldsymbol{B}_k^{2-} \underline{\boldsymbol{q}}_{k+1}^{S-} + \boldsymbol{B}_k^{2+} \underline{\boldsymbol{q}}_{k+1}^{S+} \big)\big)^4 \ \wedge \\
&\qquad \boldsymbol{P}_z^{\mp}(t_k) (\tilde{\boldsymbol{T}}_{z,k+1}^{\mp})^4 \ \leq\ \overline{\boldsymbol{q}}_{k+1}^{S\mp} - \boldsymbol{P}_s^{\mp}(t_k) \big(\boldsymbol{M}^{\mp} \big(\boldsymbol{A}_k \boldsymbol{X}_k + \ldots \\
&\qquad\qquad \ldots\ \boldsymbol{B}_k^{1-} \boldsymbol{q}_k^{1-} + \boldsymbol{B}_k^{1+} \boldsymbol{q}_k^{1+} + \boldsymbol{B}_k^{2-} \overline{\boldsymbol{q}}_{k+1}^{S-} + \boldsymbol{B}_k^{2+} \overline{\boldsymbol{q}}_{k+1}^{S+} \big)\big)^4 \ \wedge \\
&\qquad (\underline{\boldsymbol{T}}_{z,k+1}^{\mp})^4 \ \leq\ (\tilde{\boldsymbol{T}}_{z,k+1}^{\mp})^4 \ \leq\ (\overline{\boldsymbol{T}}_{z,k+1}^{\mp})^4
\end{aligned}
\tag{18}
$$

This expression merely constitutes a *quadratic optimization problem with linear constraints* for which efficient algorithms are readily available (cf. [41–45]). Here, the Matlab® command `quadprog` is used for solving the problem *separately* for the bottom and the top half of the furnace. From the optimal solution $\tilde{\boldsymbol{T}}_{z,k+1}^{\mp}$, the component $\tilde{T}_{z,1,k+1}^{\mp}$ is simply discarded to obtain $\tilde{\boldsymbol{T}}_{zc,k+1}^{\mp}$.

Using diagonal matrices $\boldsymbol{W}_{k+1}^{-} = \boldsymbol{W}_{k+1}^{+}$, $\boldsymbol{W}_{k+1}^{\Delta_t -} = \boldsymbol{W}_{k+1}^{\Delta_t +}$, and $\boldsymbol{W}_{k+1}^{\Delta_z -} = \boldsymbol{W}_{k+1}^{\Delta_z +}$ proved useful. The time dependency of $\boldsymbol{W}_{k+1}^{\mp}$ is designed to penalize the deviation $(q_{j,k+1}^{1\mp} - \tilde{q}_{j,k+1}^{1\mp})^2$ more as the exit time $t_{j,exit}$ of the respective slab j draws nearer. Moreover, $\boldsymbol{W}_{k+1}^{\mp}$ should account for the monetary value of the slabs, as reflected by w_j from Table 1. Expanding the cost function in (18) would allow the incorporation of additional control objectives, e. g., shifting the bulk heat input towards the end of the furnace, which improves energy efficiency [3, 9, 15, 20, 21].

4.3.4. Inequality constraints

The bounds $\underline{\boldsymbol{q}}_{j,k+1}^{S\mp}$ and $\overline{\boldsymbol{q}}_{j,k+1}^{S\mp}$ may be so restrictive that a solution of (18) is *not* feasible. Therefore, if a numerical algorithm fails to solve (18), some (low-priority) constraints are expanded or given up. The strategy is implemented as follows: Recurrently expand the limits $\underline{\boldsymbol{q}}_{k+1}^{S\mp}$ and $\overline{\boldsymbol{q}}_{k+1}^{S\mp}$ by

$$
\underline{\boldsymbol{q}}_{k+1}^{S\mp} = (\boldsymbol{I} - \mathrm{diag}\{\underline{\boldsymbol{\alpha}}\}) \underline{\boldsymbol{q}}_{k+1}^{S\mp} + \mathrm{diag}\{\underline{\boldsymbol{\alpha}}\} \underline{\boldsymbol{q}}_{k+1}^{H\mp}, \qquad \overline{\boldsymbol{q}}_{k+1}^{S\mp} = (\boldsymbol{I} - \mathrm{diag}\{\overline{\boldsymbol{\alpha}}\}) \overline{\boldsymbol{q}}_{k+1}^{S\mp} + \mathrm{diag}\{\overline{\boldsymbol{\alpha}}\} \overline{\boldsymbol{q}}_{k+1}^{H\mp}
$$

until a solution of (18) is feasible. The vectors $\underline{\boldsymbol{\alpha}}$, $\overline{\boldsymbol{\alpha}} \in (0,1]^{N_s}$ contain user-defined adaptation parameters, which are usually significantly smaller than unity. Their selection takes into account the weighting factors w_j from Table 1.

4.4. Step 1c - Forward integration

Once the optimal inputs $\tilde{\boldsymbol{T}}_{zc,k+1}^{\mp}$ are known, the unknown new system states $\boldsymbol{X}_{k+1}$ are computed by forward integration of the model (3) and (6) with $\tilde{\boldsymbol{T}}_{zc,k+1}^{\mp}$ from step 1b. $\boldsymbol{X}_{k+1}$ will be used mainly in the control laws (12) (step 1a) and the optimization problem (18) (step 1b) when planning the trajectories at the subsequent sampling point.

The actual calculation of $\boldsymbol{X}_{k+1}$ proceeds as follows: (3) is specialized for $t = t_{k+1}$ and plugged into (6). Utilizing (4) and given that $\boldsymbol{X}_k$, $\boldsymbol{q}_k^{1\mp}$, and $\boldsymbol{T}_{zc,k+1}^{\mp} = \tilde{\boldsymbol{T}}_{zc,k+1}^{\mp}$ are known, an implicit nonlinear equation for $\boldsymbol{X}_{k+1}$ is obtained. It can be solved by means of the *Newton-Raphson method*, which exhibits quadratic

Post-print version of the article: A. Steinboeck, K. Graichen, D. Wild, T. Kiefer, and A. Kugi, "Model-based trajectory planning, optimization, and open-loop control of a continuous slab reheating furnace", *Journal of Process Control*, vol. 21, no. 2, pp. 279–292, 2011. DOI: 10.1016/j.jprocont.2010.08.004

convergence. It is emphasized that many approximations adopted in the steps 1a and 1b, e. g., (8), are not needed here.

If the end of the planning period $[t_{k_0}, t_{k_1}]$ is reached, i. e., if $t_{k+1} = t_{k_1}$, the algorithm proceeds with step 2, otherwise with step 1a.

4.5. Step 2 - Rescaling

Generally, the expected trajectories $(\boldsymbol{x}_{j,k})$ will deviate from the reference values $(\tilde{\boldsymbol{x}}_{j,k})$, especially, after the first iteration loop. It is a reasonable assumption that $(\boldsymbol{x}_{j,k})$ is a more realistic trajectory than $(\tilde{\boldsymbol{x}}_{j,k})$. In contrast to $(\tilde{\boldsymbol{x}}_{j,k})$, $(\boldsymbol{x}_{j,k})$ is a solution of (3) and (6) with the inputs $(\tilde{\boldsymbol{T}}^{\mp}_{zc,k})$. Therefore, the previous reference trajectories $(\tilde{\boldsymbol{x}}_{j,k})$ are replaced with the expected trajectories $(\boldsymbol{x}_{j,k})$. Since the final state $\boldsymbol{x}_{j,end} = \boldsymbol{x}_j(t_{j,exit})$ will deviate from its desired value $\tilde{\boldsymbol{x}}_{j,end}$, $(\boldsymbol{x}_{j,k})$ is rescaled such that $\boldsymbol{x}_{j,end} = \tilde{\boldsymbol{x}}_{j,end}$, i. e.,

$$(\tilde{\boldsymbol{x}}_{j,k}) = (\boldsymbol{x}_{j,k} + \tau_j(t_k)(\tilde{\boldsymbol{x}}_{j,end} - \boldsymbol{x}_{j,end})) \tag{19}$$

with $\tau_j(t)$ from (7).

Given that the achieved planning results $(\boldsymbol{x}_{j,k})\ \forall j \in J$ and $(\tilde{\boldsymbol{T}}^{\mp}_{zc,k})$ are *good* enough, the planning algorithm terminates at this point. Otherwise, it restarts at step 1a. In practical terms, it proved sufficient to stop after the first or second iteration loop.

5. Example problem

The control scheme has been tested in a simulation environment, which contains the comprehensive furnace model [34] and an emulator of the low-level zone temperature controllers (inner loop shown in Figure 3). The inner loop was simply provided with reference signals $(\tilde{\boldsymbol{T}}^{\mp}_{zc,k})$ from the trajectory planning algorithm.

On a standard PC (2.4 GHz, 2 GB RAM), an implementation of the algorithm in MATLAB® requires less than 0.5 s CPU time for planning 1 h of furnace operation with sampling periods $\Delta t_k < 2$ min. This is tantamount to 12 s CPU time for planning one full day of operation. As demonstrated in [36], the computational effort can be further reduced if the sampling period Δt_k is increased.

5.1. Problem formulation

Figure 6 shows a test scenario with 198 slabs being processed during 68 h of furnace operation. At the beginning, slabs with $D_j = 0.15$ m and $W_j = 1.98$ m are reheated to a desired final temperature $\tilde{T}_{j,end} = 1400$ K within 5 h. Later, the thickness undergoes a step such that $D_j = 0.4$ m holds for all slabs withdrawn later than $t = 12$ h (cf. Figure 6a)). The furnace is 35.1 m long and contains 18 slabs at a time.

Starting at $t = 24$ h (slab $j = 87$, cf. Figure 6b)), the reheating time of the slabs is gradually increased up to 7 h (slab $j = 105$), which is a reasonable value for slabs of this thickness. Figure 6c) shows representative path-time diagrams. To avoid clutter, only every second slab is embodied in the plot. The slabs $j = 1$ through $j = 87$ exhibit an identical yet time-shifted path-time diagram. The same holds true for the slabs $j = 105$ through $j = 198$.

The test scenario proceeds with variations in the desired final slab temperature. At $t = 36$ h, $\tilde{T}_{j,end}$ steps from 1400 K to 1460 K. Between $t = 48$ h and $t = 57$ h, $\tilde{T}_{j,end}$ is ramped down and up again with a temperature difference of 10 K with respect to the previous slab (cf. Figure 6d)). The slabs enter the furnace with an initial temperature of $T_{j,0} = 380$ K, because they are already heated when waiting in front of the furnace.

Post-print version of the article: A. Steinboeck, K. Graichen, D. Wild, T. Kiefer, and A. Kugi, "Model-based trajectory planning, optimization, and open-loop control of a continuous slab reheating furnace", *Journal of Process Control*, vol. 21, no. 2, pp. 279–292, 2011. DOI: 10.1016/j.jprocont.2010.08.004
The content of this post-print version is identical to the published paper but without the publisher's final layout or copy editing.

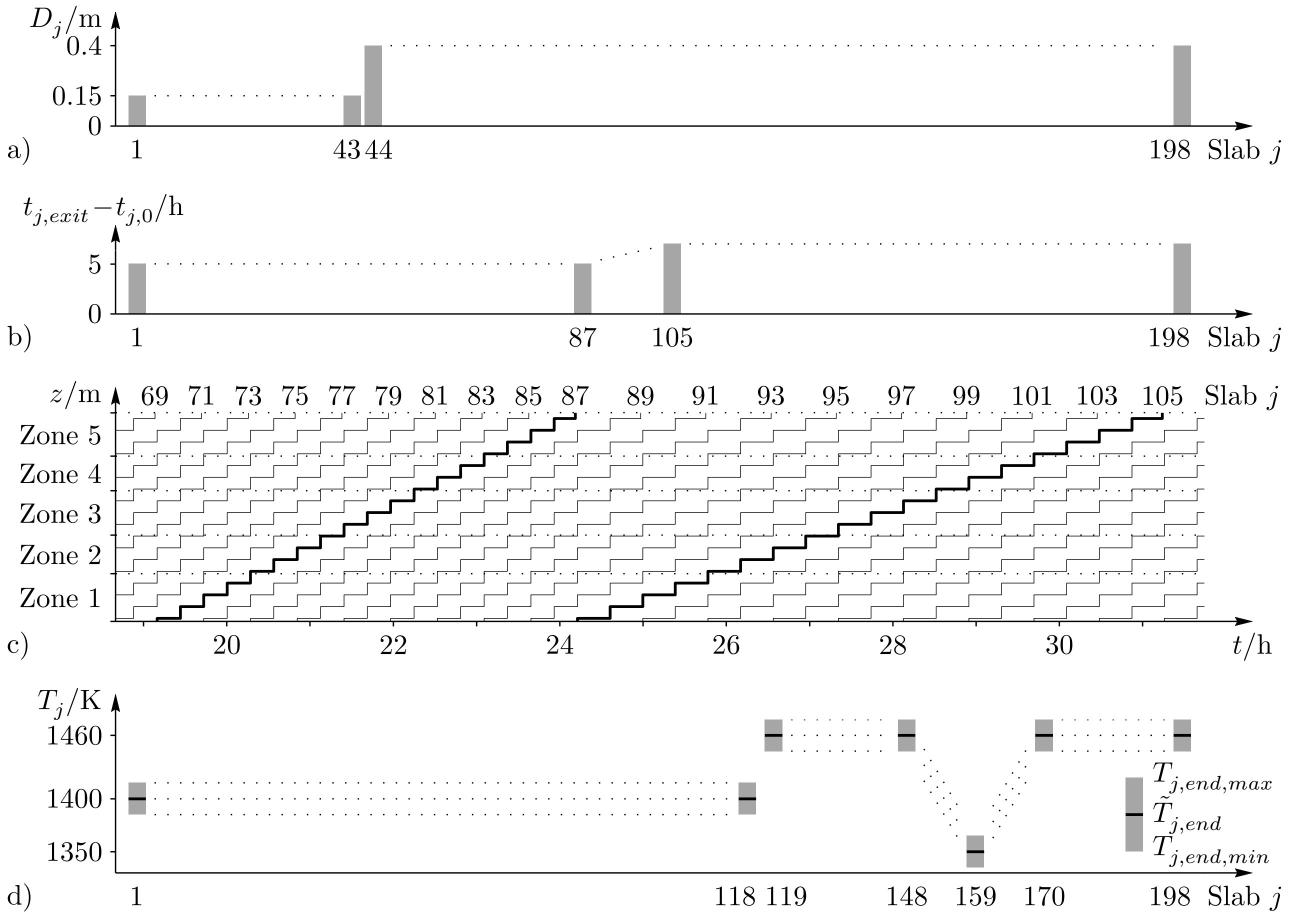

Figure 6: Overview of slab schedule, a) slab thickness, b) residence time of the slab inside the furnace, c) path-time diagrams, d) desired final slab temperature profile.

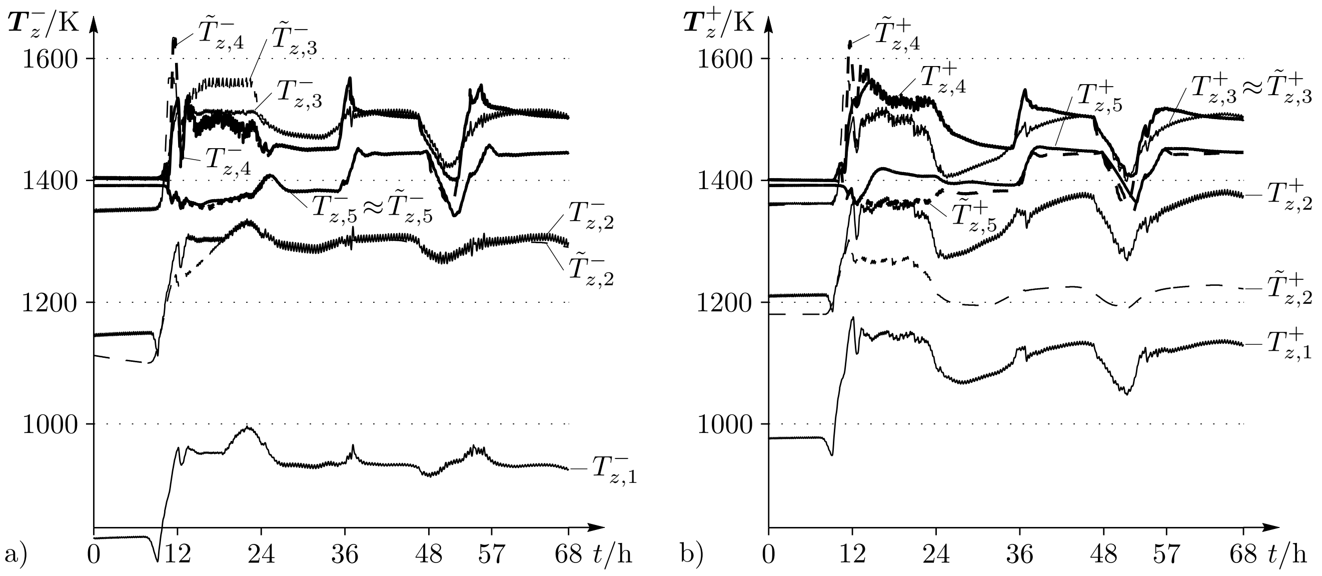

Figure 7: Planned and simulated furnace zone temperatures, a) bottom half of the furnace, b) top half of the furnace.

To keep the scenario as simple as possible, all slabs have the same width W_j, the same weighting factor

Post-print version of the article: A. Steinboeck, K. Graichen, D. Wild, T. Kiefer, and A. Kugi, "Model-based trajectory planning, optimization, and open-loop control of a continuous slab reheating furnace", *Journal of Process Control*, vol. 21, no. 2, pp. 279–292, 2011. DOI: 10.1016/j.jprocont.2010.08.004
The content of this post-print version is identical to the published paper but without the publisher's final layout or copy editing.

w_j, and the same material. The temperature-dependent material parameters c_j and λ_j are taken from [36, Figure 2]. Constraints on the slab temperature trajectory (cf. Appendix B.2.2) were chosen as $T_{j,homo,min} = T_{j,end,min} = \tilde{T}_{j,end} - 15\,\mathrm{K}$ with $t_{j,homo} = 0.67\,\mathrm{h}$, $T_{j,end,max} = \tilde{T}_{j,end} + 15\,\mathrm{K}$, $T_{j,abs,max} = \tilde{T}_{j,end} + 100\,\mathrm{K}$, $\Delta T_{j,max} = D_j 1500\,\mathrm{K/m}$, and $\Delta T_{j,end,max} = T_{j,end,max} - T_{j,end,min} = 30\,\mathrm{K}$.

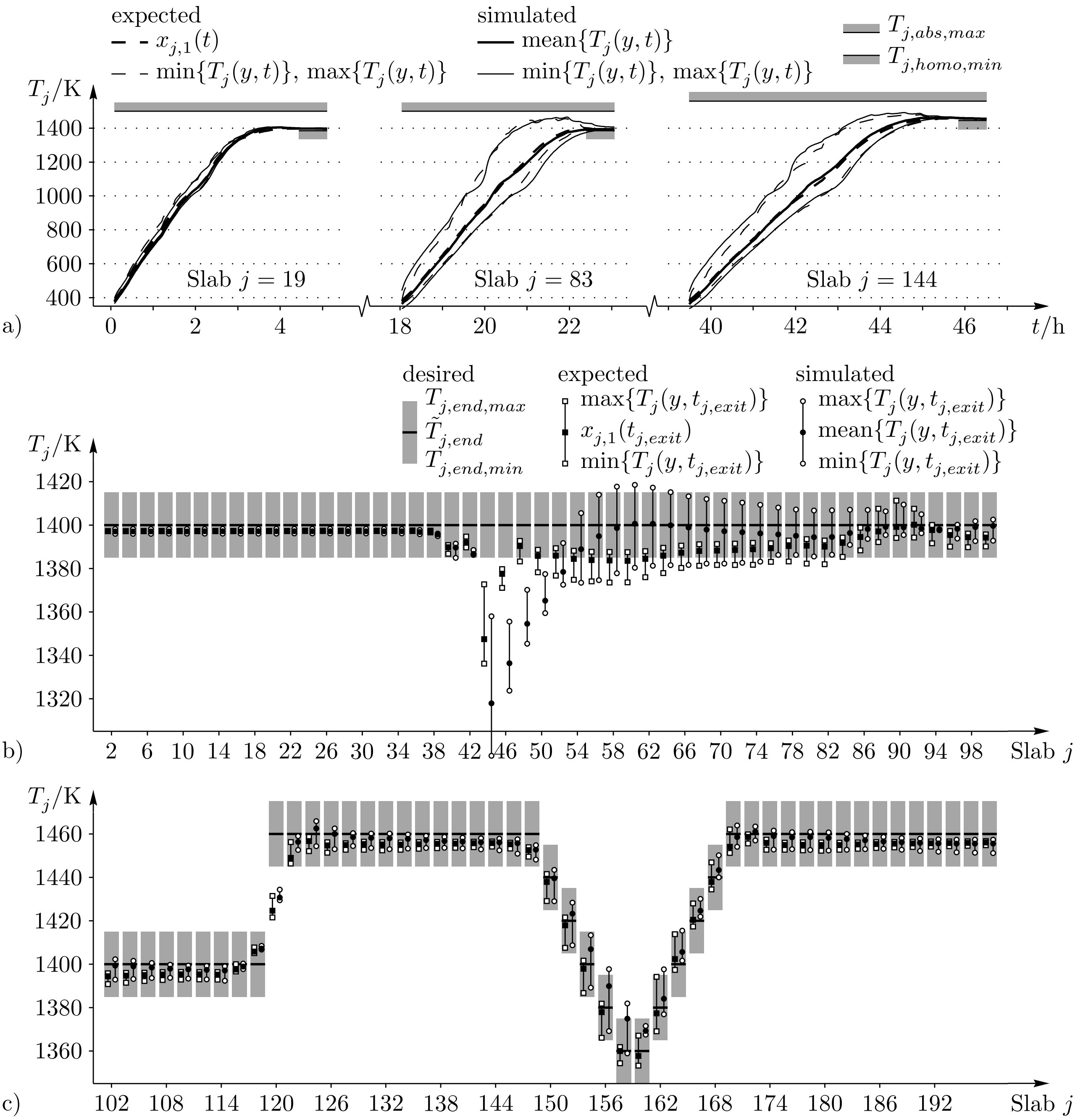

Figure 8: Expected and simulated slab temperatures, a) representative slab temperature trajectories, b) final slab temperatures, c) final slab temperatures (continued).

5.2. Furnace zone temperatures

Figure 7 shows the planned reference zone temperature (dashed lines) together with the simulated values (solid lines). These trajectories are subject to constraints—not shown in Figure 7—in terms of both value

Post-print version of the article: A. Steinboeck, K. Graichen, D. Wild, T. Kiefer, and A. Kugi, "Model-based trajectory planning, optimization, and open-loop control of a continuous slab reheating furnace", *Journal of Process Control*, vol. 21, no. 2, pp. 279–292, 2011. DOI: 10.1016/j.jprocont.2010.08.004

and gradient (cf. (14)). The control errors are mainly caused by limitations of the fuel flow rates which are considered only by the comprehensive model. That means, the zone temperature controllers are not always capable of exactly following the commanded trajectories ($\tilde{\boldsymbol{T}}^{\mp}_{zc,k}$), even if they conform to the constraints (14). Zone 2 in the top half of the furnace is a typical example for this problem. There, the burners practically always operate at minimum output. Results for the slab reheating curves obtained with the zone temperatures from Figure 7 are discussed in the sequel.

5.3. Slab temperatures

Temperature trajectories of three representative slabs are provided in Figure 8a). The mean temperatures are plotted as thick lines, whereas the thin lines correspond to the minimum and the maximum slab temperatures. Results from the trajectory planning process, based on the reduced model, are displayed as dashed graphs. Note that here the expected reheating trajectories, i. e., those before the last rescaling operation in step 2 (cf. Figure 4), are given. The solid curves are the simulation results from the comprehensive model [34].

Neither the hard constraint $\Delta T_{j,max}$ (cf. (22a)) nor the hard upper limit $T_{j,abs,max}$ (cf. (21b)) is exceeded by any slab, which is also corroborated by Figure 8a). For the thin slabs ($D_j = 0.15\,\mathrm{m}$) a reheating time of 5 h is almost too long, as may be inferred from the trajectory of slab $j = 19$. Other simulations have shown that already a reheating time of 2.2 h suffices for these slabs.

The final slab temperature profile of every second slab is shown in Figure 8b) and c). Expected values from the reduced model are marked with squares, whereas circles represent results of the comprehensive model. Once again, it is confirmed that reheating thin slabs ($D_j = 0.15\,\mathrm{m}$) is not a difficult task.

At the transition from thin to thick slabs (around $t = 12\,\mathrm{h}$) some slabs leave the furnace at too low temperatures, because the dynamics of the furnace does not permit such abrupt changes of the slab thickness. Hence, for the real furnace operation, it seems expedient to change the slab geometry only gradually. Although the slabs $j = 56$ through $j = 91$ more or less reach their desired final mean temperature, the time for homogenizing their temperature profiles is insufficient (cf. Figure 8b)). The lower constraint $T_{j,homo,min}$ (cf. (21c)) is violated for these slabs, as illustrated in Figure 8a) for slab $j = 83$. From slab $j = 92$ onward (until $j = 118$), all constraints of the slab temperature trajectory are satisfied. Slab $j = 92$ stays in the furnace for 5.6 h.

At $t = 36\,\mathrm{h}$, the desired final slab temperature takes a considerable leap—a scenario which should be avoided in the real process. Here, 3 slabs ($j = 119$, 120, and 121) miss their desired final temperature range $[T_{j,end,min}, T_{j,end,max}]$ and the lower bound $T_{j,homo,min}$. The situation is better, if the desired final slab temperature changes only gradually like for the slabs $j = 148$ through $j = 170$. In this case, most bounds are satisfied, except for slabs with $\tilde{T}_{j,end} \leq 1380\,\mathrm{K}$, which tend to be (moderately) too hot upon leaving the furnace. Most burners operate at their lower limit while these slabs are reheated.

The temperature trajectories in Figure 8a) exhibit a dent around the temperature $T_j = 1050\,\mathrm{K}$, which is a consequence of phase transitions of the material occurring at this temperature level. This effect is acceptably reflected in the planning process, because c_j was taken as a nonlinear function of T_j (cf. [36, Figure 2]).

There are two main reasons for slabs not meeting their control objectives: a) diversity of slab schedules, e. g., thickness or desired final temperature may vary considerably between neighboring slabs, and b) limitations of manipulated variables (fuel flow rates). The problem a) can be alleviated by designing less demanding slab schedules, whereas the issue b) characterizes a principal shortcoming of many hierarchical control structures.

6. Conclusion

A trajectory planning and optimization algorithm for non-steady-state operation of a slab reheating furnace was developed. The model-based control approach plans furnace zone temperatures ($\tilde{\boldsymbol{T}}^{\mp}_{zc,k}$), which serve as reference signals for low-level controllers governing the fuel and air supply of multiple burners.

Post-print version of the article: A. Steinboeck, K. Graichen, D. Wild, T. Kiefer, and A. Kugi, "Model-based trajectory planning, optimization, and open-loop control of a continuous slab reheating furnace", *Journal of Process Control*, vol. 21, no. 2, pp. 279–292, 2011. DOI: 10.1016/j.jprocont.2010.08.004
The content of this post-print version is identical to the published paper but without the publisher's final layout or copy editing.

The considered plant is nonlinear, time-variant, and the control inputs as well as the system states are constrained.

The outlined algorithm materializes an iterative two-step approach. In step 1, desired heat inputs $\tilde{\boldsymbol{q}}^{1\mp}_{k+1}$ into the slabs are individually designed by SISO feedback control of Galerkin coefficients of the simulation model. These states are subject to several soft and hard constraints defining the slab reheating quality. Moreover, zone temperatures $\tilde{\boldsymbol{T}}^{\mp}_{zc,k+1}$ are computed for the whole system by means of a quadratic program to achieve an optimum realization of the desired values $\tilde{\boldsymbol{q}}^{1\mp}_{k+1}$. In step 2 of the algorithm, the expected slab temperature trajectories are rescaled such that the final temperature profile exactly matches the desired value.

The feasibility of the method was demonstrated by means of an example problem simulated with the validated furnace model [34]. The most salient advantages of the approach are:

- Constraints on both the furnace operation and the slab reheating trajectories are adequately reflected.
- The method accounts for radiative interaction within the whole furnace and is, thus, not restricted to controlling a single zone.
- Optimal slab reheating trajectories are generated for each individual slab, i. e., they are not parameterized in terms of slab location or furnace zone.
- The algorithm is suitable for planning non-steady-state furnace operation, meaning that the slabs may vary significantly in terms of their desired final temperature and other properties.
- The method always furnishes a solution, i. e., problems with unfeasible planning results are effectively remedied.
- The approach manages without heavy mathematics or control theory and is, therefore, computationally undemanding. Employing a standard PC, one full day of furnace operation can be planned within 12 s, which renders the scheme suitable for both offline and online trajectory planning.
- The algorithm exhibits linear time complexity with respect to the length of the planning period $[t_{k_0}, t_{k_1}]$ and also with respect to the total number of slabs.
- It is a *stand-alone* algorithm, insofar as interfaces to measurement devices, observers, or downstream control entities are not required. Thus, the method is suitable for preplanning and open-loop control.

The proposed algorithm furnishes reference signals which may be utilized in feedback control, e. g., in a two-degrees-of-freedom control scheme. It is likely that this would further improve the reheating quality of the slabs. Consequently, future research should focus on developing a MIMO state feedback law. Also, implementing the planning algorithm in the high-level controller of a real furnace system is envisaged for the near future. Bearing in mind the high accuracy of the comprehensive model (cf. [34]), it is expected that the presented results can be reproduced in reality.

Acknowledgments

The authors from Vienna University of Technology highly appreciate the ongoing technical expertise and the financial support provided by AG der Dillinger Hüttenwerke.

Post-print version of the article: A. Steinboeck, K. Graichen, D. Wild, T. Kiefer, and A. Kugi, "Model-based trajectory planning, optimization, and open-loop control of a continuous slab reheating furnace", *Journal of Process Control*, vol. 21, no. 2, pp. 279–292, 2011. DOI: 10.1016/j.jprocont.2010.08.004

References

[1] D. G. Carpenter, C. W. Proctor, Temperature control and optmization of a reheat furnace using a distributed control system, Iron and Steel Engineer 64 (8) (1987) 44–49.

[2] S. Chen, S. Abraham, D. Poshard, Modification of reheat furnace practices through comprehensive process modeling, Iron & Steel Technology 5 (8) (2008) 66–79.

[3] P. Fontana, A. Boggiano, A. Furinghetti, G. Cabras, C. A. Simoncini, An advanced computer control system for reheat furnaces, Iron and Steel Engineer 60 (8) (1983) 55–62.

[4] F. Hollander, S. P. A. Zuurbier, Design, development and performance of online computer control in a 3-zone reheating furnace, Iron and Steel Engineer 59 (1) (1982) 44–52.

[5] M. Honner, Z. Vesely, M. Svantner, F. Cejka, Optimal heating control system for continuous furnaces, Industrial Heat Engineering 23 (3) (2001) 105–111.

[6] B. Leden, A control system for fuel optimization of reheating furnaces, Scandinavian Journal of Metallurgy 15 (1986) 16–24.

[7] P. Marino, A. Pignotti, D. Solis, Control of pusher furnaces for steel slab reheating using a numerical model, Latin Amercian Applied Research 34 (4) (2004) 249–255.

[8] L. Rixin, N. Baolin, Mathematical model for dynamic operation and optimum control of pusher type slab reheating furnace, Industrial Heating 59 (3) (1992) 60–62.

[9] F. Shenvar, Walking beam furnace supervisory control at inland's 80-in. hot strip mill, Iron and Steel Engineer 71 (7) (1994) 25–34.

[10] D. Staalman, The funnel model for accurate slab temperature in reheating furnaces, La Revue de Métallurgie 101 (7) (2004) 453–459.

[11] F. Vode, A. Jaklič, T. Kokalj, D. Matko, A furnace control system for tracing reference reheating curves, Steel Research International, Metal Forming 79 (5) (2008) 364–370.

[12] D. Wild, T. Meurer, A. Kugi, O. Fichet, K. Eberwein, Nonlinear observer design for pusher-type reheating furnaces, Proceedings of the 3rd International Steel Conference on New Developments in Metallurgical Process Technologies, Düsseldorf, Germany (2007) 790–797.

[13] L. Croce, A. Grosse-Gorgemann, New aspects in controlling a reheating furnace for slabs by a thermodynamic model, Proceedings of the 2nd International Conference of Simulation & Modeling of Metallurgical Processes in Steelmaking, STEELSIM, Graz, Austria (2007).

[14] J. L. Roth, H. Sierpinski, J. Chabanier, J. M. Germe, Computer control of slab furnaces based on physical models, Iron and Steel Engineer 63 (8) (1986) 41–47.

[15] R. J. Schurko, C. Weinstein, M. K. Hanne, D. J. Pellecchia, Computer control of reheat furnaces: A comparison of strategies and applications, Iron and Steel Engineer 64 (5) (1987) 37–42.

[16] T. A. Veslocki, C. S. Smith, C. D. Kelly, Automatic slab heating control at Inland's 80-in. hot strip mill, Association of Iron and Steel Engineers (AISE) Year Book (1986) 577–584.

[17] M. K. F. Knoop, J. A. Moreno Pérez, Nonlinear PI-controller design for a continuous-flow furnace via continuous gain scheduling, Journal of Process Control 4 (3) (1994) 143–147.

[18] L. Balbis, J. Balderud, M. J. Grimble, Nonlinear predictive control of steel slab reheating furnace, Proceedings of the American Control Conference, Seattle, Washington, USA (2008) 1679–1684.

[19] A. Schutti, E. Schiller, A. Ortner, M. Rosenthaler, D. Auzinger, M. Lichtenwagner, G. Mitter, Neues Konzept zur Prozessführung der Stoßöfen von voestalpine Stahl, Stahl und Eisen 124 (10) (2004) 43–50.

[20] R. Westdorp, Development and simulation of a control strategy for a reheating furnace, Journal A 29 (2) (1988) 11–16.

[21] H. Ezure, Y. Seki, N. Yamaguchi, H. Shinonaga, Development of a simulator to calculate an optimal slab heating pattern for reheat furnaces, Electrical Engineering in Japan 120 (3) (1997) 42–53.

[22] Z. Wang, T. Chai, S. Guan, C. Shao, Hybrid optimization setpoint strategy for slab reheating furance temperature, Proceedings of the American Control Conference, San Diego, California (1999) 4082–4086.

[23] A. H. Wörk, Optimal control of slab reheating furnaces, Proceedings of the IFAC Symposion on the control of distributed parameter systems, Banff, Alberta, Canada I (1971).

[24] B. Dahm, R. Klima, Feedback control of stock temperature and oxygen content in reheating furnaces, Proceedings of the IOM Conference on Challenges in Reheating Furnaces, London, UK (2002) 287–296.

[25] G. v. Ditzhuijzen, D. Staalman, A. Koorn, Identification and model predictive control of a slab reheating furnace, Proceedings of the 2002 IEEE International Conference on Control Applications, Glasgow, UK (2002) 361–366.

[26] Z. A. Icev, J. Zhao, M. J. Stankovski, T. D. Kolemisevska-Gugulovska, G. M. Dimirovski, Supervisory-plus-regulatory control design for efficient operation of industrial furnaces, Journal of Electrical & Electronics Engineering 4 (2) (2004) 1199–1218.

[27] H. Sibarani, Y. Samyudia, Robust nonlinear slab temperature control design for an industrial reheating furnace, Computer Aided Chemical Engineering 18 (2004) 811–816.

[28] B. Zhang, Z. Chen, L. Xu, J. Wang, J. Zhang, H. Shao, The modeling and control of a reheating furnace, Proceedings of the American Control Conference, Anchorage, Alaska, USA (2002) 3823–3828.

[29] L. M. Pedersen, B. Wittenmark, On the reheat furnace control problem, Proceedings of the American Control Conference (1998) 3811–3815.

[30] R. Pichler, R. Langer, Automatisierungskonzept zur Steuerung von Öfen für Walzstraßen, Stahl und Eisen 109 (5) (1989) 239–243.

[31] H. E. Pike, S. J. Citron, Optimization studies of a slab reheating furnace, Automatica 6 (1970) 41–50.

Post-print version of the article: A. Steinboeck, K. Graichen, D. Wild, T. Kiefer, and A. Kugi, "Model-based trajectory planning, optimization, and open-loop control of a continuous slab reheating furnace", *Journal of Process Control*, vol. 21, no. 2, pp. 279–292, 2011. DOI: 10.1016/j.jprocont.2010.08.004

[32] H. S. Ko, J. Kim, T. Yoon, M. Lim, D. R. Yang, I. S. Jun, Modeling and predictive control of a reheating furnace, Proceedings of the American Control Conference, Chicago, USA 4 (2000) 2725–2729.
[33] N. Yoshitani, T. Ueyama, M. Usui, Optimal slab heating control with temperature trajectory optimization, Proceedings of the 20th International Conference on Industrial Electronics, Control and Instrumentation, IECON'94 3 (1994) 1567–1572.
[34] D. Wild, T. Meurer, A. Kugi, Modelling and experimental model validation for a pusher-type reheating furnace, Mathematical and Computer Modelling of Dynamical Systems 15 (3) (2009) 209–232.
[35] A. Steinboeck, D. Wild, T. Kiefer, A. Kugi, A mathematical model of a slab reheating furnace with radiative heat transfer and non-participating gaseous media, International Journal of Heat and Mass Transfer, in press (2010) http://dx.doi.org/10.1016/j.ijheatmasstransfer.2010.07.029.
[36] A. Steinboeck, D. Wild, T. Kiefer, A. Kugi, A flexible time integration method for the 1D heat conduction problem, Proceedings of the 6th Vienna Conference on Mathematical Modelling, Vienna, Austria, ARGESIM Report no. 35 (2009) 1204–1214.
[37] H. D. Baehr, K. Stephan, Heat and Mass Transfer, 2nd Edition, Springer-Verlag, Berlin Heidelberg, 2006.
[38] F. P. Incropera, D. P. DeWitt, T. L. Bergman, A. S. Lavine, Fundamentals of Heat and Mass Transfer, 6th Edition, J. Wiley & Sons, Hoboken, NJ, 2007.
[39] J. H. Lienhard IV, J. H. Lienhard V, A Heat Transfer Textbook, 3rd Edition, Phlogiston Press, Cambridge, Massachusetts, 2002.
[40] M. F. Modest, Radiative Heat Transfer, 2nd Edition, Academic Press, New York, 2003.
[41] S. Boyd, L. Vandenberghe, Convex Optimization, Cambridge University Press, Cambridge, UK, 2004.
[42] R. Fletcher, Practical methods of optimization, 2nd Edition, J. Wiley & Sons, Chichester, New York, 1987.
[43] P. E. Gill, W. Murray, M. H. Wright, Practical Optimization, Academic Press, London, 1981.
[44] D. G. Luenberger, Optimization by Vector Space Methods, Wiley-Interscience, New York, 1969.
[45] J. Nocedal, S. J. Wright, Numerical Optimization, 2nd Edition, Springer Series in Operations Research, Springer, New York, 2006.

A. Mapping matrices of the radiative heat exchange law

The matrices $\boldsymbol{P}_z^{\mp} = [P_{z,i,j}^{\mp}]_{i=j_{start}\cdots j_{end},j=1\ldots N_z^{\mp}}$ and $\boldsymbol{P}_s^{\mp} = [P_{s,i,j}^{\mp}]_{i=j_{start}\cdots j_{end},j=j_{start}\cdots j_{end}}$ used in (3) are straightforward results of the net radiation method [37–40] (see also [35]). They depend on the geometry and the radiative properties of the participating surfaces. Flue gases are considered as transparent. $\boldsymbol{P}_z^{\mp}$ and $\boldsymbol{P}_s^{\mp}$ are piecewise constant with respect to t; in fact, they are constant during each period $[t_l^s, t_{l+1}^s)$. At any time,

$$0 \leq P_{z,i,j}^{\mp} < \sigma, \qquad |P_{s,i,j}^{\mp}| < \sigma,$$

$$P_{s,i,j}^{\mp} \begin{cases} \geq 0 & \text{if } i \neq j \\ < 0 & \text{else} \end{cases}, \qquad \sum_{j=j_{start}}^{j_{end}} P_{s,i,j}^{\mp} < 0, \qquad \sum_{j=1}^{N_z^{\mp}} P_{z,i,j}^{\mp} + \sum_{j=j_{start}}^{j_{end}} P_{s,i,j}^{\mp} = 0,$$

where σ is the Stefan-Boltzmann constant. Generally, $P_{z,i,j}^{\mp}$ and $P_{s,i,j}^{\mp}$ are unequal to zero. The above expressions confirm that (cf. [35])

- $q_j^{\mp}(t)\ \forall\, j \in J$ is monotonically *non-decreasing* with $\begin{bmatrix} 1 & \mp 1 & 2/3 \end{bmatrix} \boldsymbol{x}_i(t)\ \forall\, i \in J,\, i \neq j$,
- $q_j^{\mp}(t)\ \forall\, j \in J$ is monotonically *non-rising* with $\begin{bmatrix} 1 & \mp 1 & 2/3 \end{bmatrix} \boldsymbol{x}_j(t)$, and
- $q_j^{\mp}(t)\ \forall\, j \in J$ is monotonically *non-decreasing* with $T_{z,i}^{\mp}(t)\ \forall\, i \in \{1, 2, \ldots, N_z^{\mp}\}$.

These properties are useful for transforming between temperature bounds and constraints on $q_j^{\mp}(t)$.

B. Constraints on the slab reheating process

A furnace control algorithm should take into account that the slab reheating process is constrained by safety limits and physical restrictions. For convenience, the constraints summarized in this section are given for the continuous-time domain only.

Post-print version of the article: A. Steinboeck, K. Graichen, D. Wild, T. Kiefer, and A. Kugi, "Model-based trajectory planning, optimization, and open-loop control of a continuous slab reheating furnace", *Journal of Process Control*, vol. 21, no. 2, pp. 279–292, 2011. DOI: 10.1016/j.jprocont.2010.08.004
The content of this post-print version is identical to the published paper but without the publisher's final layout or copy editing.

B.1. Constraints on the furnace zone temperatures

The fuel flow rates to the burners are restricted by both lower bounds (considerably above zero) and upper bounds. These narrow limits constrain the zone temperatures, which can be formulated as

$$T^{\mp}_{z,i,min}(t) \leq T^{\mp}_{z,i}(t) \leq T^{\mp}_{z,i,max}(t), \quad \dot{T}^{\mp}_{z,i,min}(t) \leq \dot{T}^{\mp}_{z,i}(t) \leq \dot{T}^{\mp}_{z,i,max}(t) \quad \forall\, i \in \{1, 2, \ldots, N^{\mp}_z\}. \tag{20}$$

Moreover, the constraints $T^{\mp}_{z,i,max}(t)$, $\dot{T}^{\mp}_{z,i,min}(t)$, and $\dot{T}^{\mp}_{z,i,max}(t)$ protect the furnace against thermal or thermomechanical damages.

Most of the time, $T^{\mp}_{z,i,min}(t)$, $T^{\mp}_{z,i,max}(t)$, $\dot{T}^{\mp}_{z,i,min}(t)$, and $\dot{T}^{\mp}_{z,i,max}(t)$ can be assumed as constant, which, however, neglects the influence of the slabs on the zone temperatures. For trajectory planning, time-variant design of the limits (cf. (14)) is a flexible and 'safe' way of user intervention into the control algorithm. For instance, it allows prescribing the temperature in some zones and may be used for manual shut down, start up, or production halts of the furnace. User interventions generally force the planning algorithm to deviate from the optimal trajectories, which can affect the reheating quality of the slabs. The next subsection outlines how the reheating quality may be defined.

B.2. Constraints on the slab temperatures

Only a single slab j is considered in this subsection. The high-priority objective that each slab reaches its desired final temperature is supplemented by restrictions on the slab temperature profile. For convenience, these restrictions will be expressed in terms of the state $\boldsymbol{x}_j(t)$.

B.2.1. Operators

Let the binary operator $\preccurlyeq$ $(\succcurlyeq) : \mathbb{R}^3 \times \mathbb{R}^3 \to \{0, 1\}$ be defined as

$$\boldsymbol{x}_1 \overset{(\succcurlyeq)}{\preccurlyeq} \boldsymbol{x}_2 \quad \Leftrightarrow \quad \begin{bmatrix} 1 & \eta & \eta^2 - 1/3 \end{bmatrix} (\boldsymbol{x}_2 - \boldsymbol{x}_1) \overset{(\leq)}{\geq} 0 \qquad \forall\, \eta \in (-1, 1)$$

with some arbitrary states $\boldsymbol{x}_1$ and $\boldsymbol{x}_2$. This operator evaluates whether a temperature profile defined by $\boldsymbol{x}_1$ does not exceed (does not fall below) a temperature profile defined by $\boldsymbol{x}_2$. Thus, $\boldsymbol{x}_2$ and the operators $\preccurlyeq$, $\succcurlyeq$ separate the space of possible states $\mathbb{R}^3$ into *closed* sets $X^+_{\boldsymbol{x}_2} = \{\boldsymbol{x}_1 \in \mathbb{R}^3 | \boldsymbol{x}_1 \succcurlyeq \boldsymbol{x}_2\}$ and $X^-_{\boldsymbol{x}_2} = \{\boldsymbol{x}_1 \in \mathbb{R}^3 | \boldsymbol{x}_1 \preccurlyeq \boldsymbol{x}_2\}$ and the remaining *open* set $X^{\sim}_{\boldsymbol{x}_2} = \mathbb{R}^3 \backslash (X^+_{\boldsymbol{x}_2} \cup X^-_{\boldsymbol{x}_2})$.

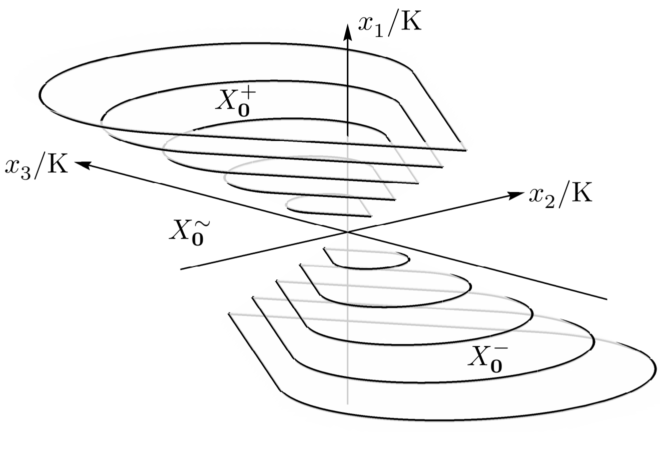

Figure 9: Partitioned space of possible temperature states (axes equally scaled).

Figure 9 shows these sets for $\boldsymbol{x}_2 = \mathbf{0}$. The corresponding sets for $\boldsymbol{x}_2 \neq \mathbf{0}$ are found if the surface in Figure 9 is shifted by $\boldsymbol{x}_2$. Both $X^+_{\boldsymbol{x}_2}$ and $X^-_{\boldsymbol{x}_2}$ are convex sets.

Post-print version of the article: A. Steinboeck, K. Graichen, D. Wild, T. Kiefer, and A. Kugi, "Model-based trajectory planning, optimization, and open-loop control of a continuous slab reheating furnace", *Journal of Process Control*, vol. 21, no. 2, pp. 279–292, 2011. DOI: 10.1016/j.jprocont.2010.08.004
The content of this post-print version is identical to the published paper but without the publisher's final layout or copy editing.

Moreover, a unary operator $\Delta(\cdot) : \mathbb{R}^3 \to \mathbb{R}^+$ is introduced as

$$\Delta(\boldsymbol{x}) = \max_{\eta \in (-1,1)} \left\{ \begin{bmatrix} 1 & \eta & \eta^2 - 1/3 \end{bmatrix} \boldsymbol{x} \right\} - \min_{\eta \in (-1,1)} \left\{ \begin{bmatrix} 1 & \eta & \eta^2 - 1/3 \end{bmatrix} \boldsymbol{x} \right\}$$

with some state $\boldsymbol{x}$. It returns the maximum temperature difference within a slab.

B.2.2. Hard and soft constraints on the slab temperature trajectories

Slab temperatures are subject to a number of *hard* and *soft* constraints. Violating a soft constraint is only permitted if otherwise a solution is not feasible (cf. Subsections 4.3.2 and 4.3.4). The constraints may be attributed to metallurgical requirements, limited thermomechanical strength of the material, and requirements of downstream process steps.

Clearly, the final state $\boldsymbol{x}_{j,end}$ should conform to its desired value $\tilde{\boldsymbol{x}}_{j,end}$ as accurately as possible. Moreover, there is a soft lower (upper) limit $T_{j,end,min}$ ($T_{j,end,max}$) on the final slab temperature profile, i. e.,

$$\begin{bmatrix} T_{j,end,min} & 0 & 0 \end{bmatrix}^\mathsf{T} \preccurlyeq \boldsymbol{x}_{j,end} \preccurlyeq \begin{bmatrix} T_{j,end,max} & 0 & 0 \end{bmatrix}^\mathsf{T}. \tag{21a}$$

In order to avoid waste of energy as well as damage and loss of slab material, the slab temperature must obey the constant, hard upper constraint

$$\boldsymbol{x}_j(t) \preccurlyeq \begin{bmatrix} T_{j,abs,max} & 0 & 0 \end{bmatrix}^\mathsf{T} \qquad \forall\, t \in [t_{j,0}, t_{j,exit}]. \tag{21b}$$

The constant, soft lower constraint

$$\boldsymbol{x}_j(t) \succcurlyeq \begin{bmatrix} T_{j,homo,min} & 0 & 0 \end{bmatrix}^\mathsf{T} \qquad \forall\, t \in [t_{j,exit} - t_{j,homo}, t_{j,exit}] \tag{21c}$$

allows for quality standards and associated phase transitions of the material.

Large temperature differences within a slab can cause undesirable deformations, i. e., bending, or even stresses in excess of the yield strength, which itself is temperature-dependent. Therefore, the temperature inhomogeneity is subject to the constant, hard constraint

$$\Delta(\boldsymbol{x}_j(t)) \leq \Delta T_{j,max} \qquad \forall\, t \in [t_{j,0}, t_{j,exit}]. \tag{22a}$$

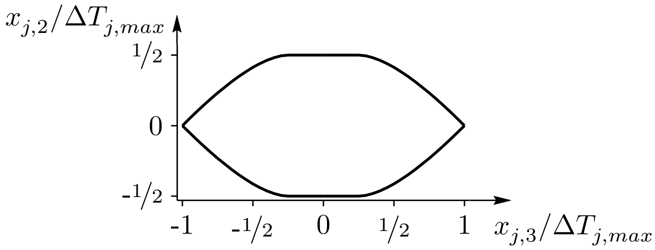

Figure 10: Constraint to avoid excessive temperature differences within a slab (axes normalized and equally scaled).

Compliance with (22a) is independent of $x_{j,1}(t)$. Hence, in the state space, the constraint spans an infinitely long cylinder centered at the axis $x_{j,1}$ (top view shown in Figure 10).

The final temperature inhomogeneity is subject to the soft constraint

$$\Delta(\boldsymbol{x}_{j,end}) \leq \Delta T_{j,end,max}, \tag{22b}$$

where $\Delta T_{j,end,max} \ll \Delta T_{j,max}$. The shape defined by (22b) is similar to the cylinder shown in Figure 10.

Post-print version of the article: A. Steinboeck, K. Graichen, D. Wild, T. Kiefer, and A. Kugi, "Model-based trajectory planning, optimization, and open-loop control of a continuous slab reheating furnace", *Journal of Process Control*, vol. 21, no. 2, pp. 279–292, 2011. DOI: 10.1016/j.jprocont.2010.08.004
The content of this post-print version is identical to the published paper but without the publisher's final layout or copy editing.

B.2.3. Merging and reformulation of constraints on the slab temperature trajectories

The above constraints can be merged for further simplification. The *hard* restrictions (21b) and (22a) constitute a *unique*, closed set

$$X_j^H = \{\, \boldsymbol{x} \in X^-_{[T_{j,abs,max}\ 0\ 0]^\mathsf{T}} \mid \Delta(\boldsymbol{x}) \leq \Delta T_{j,max} \,\}$$

of *admissible* states. Since X_j^H represents an intersection of a cone-like body as outlined in Figure 9 and a cylindrical body as outlined in Figure 10, it is convex.

A similar but time-dependent set $X_j^S(t)$ combines the *soft* constraints. It also accounts for the constraint (20) on the furnace temperatures $T^{\mp}_{z,i}(t)$. Moreover, $X_j^S(t)$ depends on the slab surface temperatures in the neighborhood of the slab j. Therefore, strictly speaking, the sets $X_j^S(t)$ should be computed for all slabs simultaneously.

However, the following approximation is made: Consider first that the heat flux densities $q_j^{\mp}(t)$ are limited because of restrictions on the slab surface temperatures and the constraints (20). Based on (3) (see also the remarks given in Appendix A) and realistic extremal slab surface temperatures, it is possible to compute non-conservative estimates $\underline{q}_j^{\mp}(t)$ and $\overline{q}_j^{\mp}(t)$ such that

$$\underline{q}_j^{\mp}(t) \leq q_j^{\mp}(t) \leq \overline{q}_j^{\mp}(t) \quad \forall\, t \in [t_{j,0}, t_{j,exit}]. \tag{23}$$

The term *non-conservative* means that (23) defines a *large* yet realistic range for $q_j^{\mp}(t)$. The limits $\underline{q}_j^{\mp}(t)$ and $\overline{q}_j^{\mp}(t)$ are computed individually for each slab and each instant $t \in [t_{j,0}, t_{j,exit}]$.

With $\underline{q}_j^{\mp}(t)$, $\overline{q}_j^{\mp}(t)$, and (1), the future restrictions (21a) and (21c) on $\boldsymbol{x}_j(t)$ can be extended backward. They are classified as *future* restrictions, because (21a) is defined at $t_{j,exit}$ and (21c) in the interval $[t_{j,exit} - t_{j,homo}, t_{j,exit}]$. Moreover, the constraints (21) are expressed as unique trajectories $\underline{\boldsymbol{x}}_j(t)$ and $\overline{\boldsymbol{x}}_j(t)$ such that for any $t_0 \in [t_{j,0}, t_{j,exit}]$

$$\underline{\boldsymbol{x}}_j(t_0) \preccurlyeq \boldsymbol{x}_j(t_0) \preccurlyeq \overline{\boldsymbol{x}}_j(t_0) \quad \Leftrightarrow \quad \exists\, (\boldsymbol{x}_j(t), q_j^{\mp}(t)) \ \ (\, (1) \wedge (21) \wedge (23)\,) \ \ \forall\, t \in [t_0, t_{j,exit}]. \tag{24}$$

The equivalence sign ($\Leftrightarrow$) ensures the uniqueness of $\underline{\boldsymbol{x}}_j(t)$ and $\overline{\boldsymbol{x}}_j(t)$.

For the constraints (22), which limit temperature inhomogeneities, a *unique* function $\overline{\Delta}_j(t) : [t_{j,0}, t_{j,exit}] \to \mathbb{R}^+$ is defined such that for any $t_0 \in [t_{j,0}, t_{j,exit}]$

$$\begin{aligned}\overline{\Delta}_j(t_0) = \max \{\, \eta \in \mathbb{R}^+ \mid \Delta(\boldsymbol{x}_j(t_0)) \leq \eta \wedge \underline{\boldsymbol{x}}_j(t_0) \preccurlyeq \boldsymbol{x}_j(t_0) \preccurlyeq \overline{\boldsymbol{x}}_j(t_0) \ \Rightarrow \\ \exists\, (\boldsymbol{x}_j(t), q_j^{\mp}(t)) \ \ (\, (1) \wedge (22) \wedge (23)\,) \ \ \forall\, t \in [t_0, t_{j,exit}] \,\}.\end{aligned}$$

Finally, $\underline{\boldsymbol{x}}_j(t)$, $\overline{\boldsymbol{x}}_j(t)$, and $\overline{\Delta}_j(t)$ yield the time-dependent set

$$X_j^S(t) = \{\, \boldsymbol{x} \in X_j^H \cap X^+_{\underline{\boldsymbol{x}}_j(t)} \cap X^-_{\overline{\boldsymbol{x}}_j(t)} \mid \Delta(\boldsymbol{x}) \leq \overline{\Delta}_j(t) \,\} \tag{25}$$

of *feasible* and *allowed* states.

Post-print version of the article: A. Steinboeck, K. Graichen, D. Wild, T. Kiefer, and A. Kugi, "Model-based trajectory planning, optimization, and open-loop control of a continuous slab reheating furnace", *Journal of Process Control*, vol. 21, no. 2, pp. 279–292, 2011. DOI: 10.1016/j.jprocont.2010.08.004

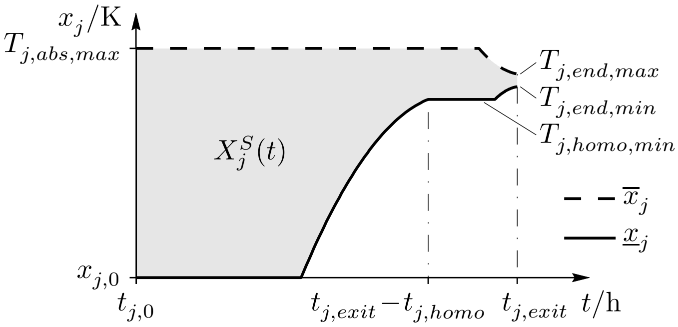

Figure 11: Set of feasible and allowed states for scalar temperature state.

For a formulation with a scalar temperature state $x_j(t)$ only, a straightforward graphical interpretation of $X_j^S(t)$ is shown in Figure 11. For a 3-dimensional state $\boldsymbol{x}_j(t)$, $X_j^S(t)$ is generated by time-variant intersections of shapes like those outlined in Figures 9 and 10.

The constraints X_j^H and $X_j^S(t)$ are *global* in the sense that they span the whole residence period $[t_{j,0}, t_{j,exit}]$ of a slab inside the furnace. They are computed *individually* for each slab and *prior* to the actual trajectory planning process.

Post-print version of the article: A. Steinboeck, K. Graichen, D. Wild, T. Kiefer, and A. Kugi, "Model-based trajectory planning, optimization, and open-loop control of a continuous slab reheating furnace", *Journal of Process Control*, vol. 21, no. 2, pp. 279–292, 2011. DOI: 10.1016/j.jprocont.2010.08.004
The content of this post-print version is identical to the published paper but without the publisher's final layout or copy editing.